Journal of Physiology (1991), **443**, *pp.* 739–777
With 9 figures
Printed in Great Britain

ACCOUNTING FOR THE Ca^{2+}-DEPENDENT KINETICS OF SINGLE LARGE-CONDUCTANCE Ca^{2+}-ACTIVATED K^+ CHANNELS IN RAT SKELETAL MUSCLE

BY O. B. McMANUS* AND K. L. MAGLEBY

From the Department of Physiology and Biophysics University of Miami School of Medicine, PO Box 016430, Miami, FL 33101, USA

(*Received 18 February 1991*)

SUMMARY

1. The Ca^{2+}-dependent kinetics of large-conductance Ca^{2+}-activated K^+ channels from cultured rat skeletal muscle were studied with the patch clamp technique. Data were collected in the absence of Na^+ and Mg^{2+}, which can alter the kinetics. About 2×10^5 open and shut intervals were analysed from each of five different excised membrane patches containing a single active channel. Analysis was restricted to activity in the normal mode, which includes 96% of the intervals.

2. The open probability (P_{open}) and dwell-time distributions of open and shut intervals were obtained at three to four different $[Ca^{2+}]_i$ for each of the channels. P_{open} data were also obtained from some multichannel patches.

3. Increasing $[Ca^{2+}]_i$ increased P_{open}. At a pH of 7·0 the Hill coefficient was $3·7 \pm 0·8$ (range of 3·0–5·0) and a P_{open} of 0·5 occurred at 14 ± 7 μM $[Ca^{2+}]_i$ ($K_{0·5}$) for data obtained at +30 mV ($n = 6$). At a pH of 7·2 the Hill coefficient was $3·0 \pm 0·5$ (range of 2·2–3·7) and $K_{0·5}$ was 9 ± 6 μM-Ca^{2+} ($n = 7$). The large standard deviations for $K_{0·5}$ reflect the observation that fourfold differences in $K_{0·5}$ could be observed for different channels studied under the same experimental conditions.

4. Hill coefficients that can be greater than 3 suggest that the channel may bind four or more Ca^{2+} to become fully activated. The binding of four Ca^{2+} before opening would require a minimum of five shut states. This estimate of the minimum number of shut states is in general agreement with that obtained from the number of exponential components in the dwell-time distributions of shut intervals. Thus, two different methods give similar estimates of the minimum number of shut states. If the channel can open with different numbers of bound Ca^{2+}, then this could give rise to the three to four open states suggested by the three to four exponential components in the open dwell-time distributions.

5. Kinetic schemes consistent with the Ca^{2+}-dependent kinetics were developed by simultaneously fitting open and shut dwell-time distributions obtained at three to four different $[Ca^{2+}]_i$, using maximum likelihood techniques and corrections for missed events. Such simultaneous fitting can provide an increased ability to define models and rate constants.

* Present address: Department of Membrane Biochemistry and Biophysics, Merck Sharp & Dohme Research Laboratories, PO Box 2000, Rahway, NJ 07065, USA.

MS 9161

6. The simplest gating mechanism that could describe the major features of the Ca^{2+}-dependence of P_{open}, the dwell-time distributions, and the relationship between the durations of the adjacent intervals was:

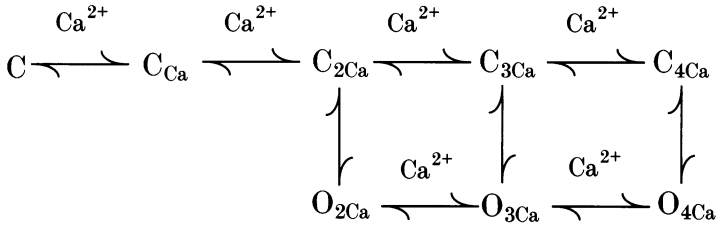

where C and O represent closed and open states, respectively. In general, the lifetimes of the shut states decrease from C to C_{3Ca}, with C_{4Ca} then increasing, and the lifetimes of the open states increase from O_{2Ca} to O_{4Ca} ($[Ca^{2+}]_i < 10$–$20\ \mu M$). The Ca^{2+} dependence of the channel arises because increasing the $[Ca^{2+}]_i$ drives the activity of the channel from the longer shut states and briefer open states towards the briefer shut states and longer open states. Models similar to the above scheme, but expanded to include six shut and four open states could improve the description of the data.

7. The effective rate constant for Ca^{2+} binding increased about 6-fold for the binding of the second Ca^{2+} and then increased another 60-fold for the binding of the third Ca^{2+}, suggesting co-operative interaction among the binding sites. Models with identical and independent Ca^{2+} bindings sites were inconsistent with the data.

8. The kinetic scheme in paragraph 6 and the expanded versions of this scheme provide working hypotheses that can describe the major features of Ca^{2+}-dependent channel gating over a 400-fold range of P_{open}.

INTRODUCTION

Large-conductance Ca^{2+}-activated K^+ channels, which are activated by micromolar concentrations of internal Ca^{2+} and by membrane depolarization, have been observed in a wide variety of tissues (Latorre, Oberhauser, Labarca & Alvarez, 1989). The unusually large conductance of these channels (200–350 pS) and high selectively for the passage of K^+ over Na^+ (Blatz & Magleby, 1984; Yellen, 1984) is consistent with their designation as BK (big K^+) or maxi K^+ channels (Latorre & Miller, 1983; Marty, 1983). The large conductance of the channel allows single-channel currents to be recorded with high resolution, and consequently, considerable progress has been made towards understanding the Ca^{2+}-dependent gating mechanism of the channel (Methfessel & Boeheim, 1982; Magleby & Pallotta, 1983*a*, *b*; Moczydlowski & Latorre, 1983). However, none of the considered models can account for the detailed kinetics of the channel, which are more complex than previously considered (McManus & Magleby, 1988). Furthermore, it is now known that dwell-time distributions obtained under a single set of experimental conditions usually contain insufficient information to adequately identify models or their rate constants (Fredkin, Montal & Rice, 1985; Blatz & Magleby, 1986*b*, 1989; Bauer, Bowman & Kenyon, 1987; Ball & Sansom, 1989; Kienker, 1989).

The purpose of this paper is to extend the kinetic analysis of large-conductance

Ca^{2+}-activated K^+ channels by analysing currents obtained at increased time resolution with more advanced techniques. The simultaneous fitting of dwell-time distributions obtained at three to four different $[Ca^{2+}]_i$ is found to provide sufficient information to identify models that can describe the major features of the Ca^{2+}-dependent kinetics of the channel. Such models have five to six shut states, three to four open states, and four to five Ca^{2+} binding sites. The proposed working hypotheses for the gating describe the Ca^{2+}-dependent shifts in the dwell-time distributions and the relationship between the durations of adjacent intervals over a 400-fold range in channel open probability. A preliminary report of the use of simultaneous fitting to identify gating mechanisms has appeared (McManus & Magleby, 1986).

METHODS

Preparation

Currents flowing through large-conductance Ca^{2+}-activated K^+ channels (Pallotta, Magleby & Barrett, 1981; Marty, 1981) in surface membranes of primary cultures of rat skeletal muscle (myotubes) were recorded with the patch clamp technique (Hamill, Marty, Neher, Sakmann & Sigworth, 1981). Pregnant rats were killed with an overdose of ether anaesthesia, and myotubes were prepared from fetal skeletal muscle as described previously (Barrett, Magleby & Pallotta, 1982). All experiments were performed on excised inside-out patches of membrane. Detailed kinetic analysis was restricted to data obtained from patches containing a single Ca^{2+}-activated K^+ channel. Single-channel patches were identified by observing openings to only a single conductance level during extended periods of recording (min) in which the open probability, P_{open}, was $> 0{\cdot}4$ (e.g. Colquhoun & Hawkes, 1990). Patches containing more than one Ca^{2+}-activated K^+ channel were unsuitable for kinetic analysis, but were sometimes used to determine the effect of $[Ca^{2+}]_i$ on channel open probability (P_{open}), since mean P_{open} is easily determined in multichannel patches (Barrett *et al.* 1982). Experiments were performed at room temperature (22–24 °C).

Solutions, recording, filtering, measuring intervals, plotting, and fitting sums of exponentials

The solutions bathing both sides of the membrane contained (mM): KCl, 144; TES buffer (*N*-tris(hydroxymethyl)methyl-2-aminoethane sulphonic acid), 2: EGTA 1, and sufficient calcium to bring the free Ca^{2+} in the solution at the inner membrane surface to the indicated levels. There was no added Ca^{2+} in the external (pipette) solution. The methods used to buffer the $[Ca^{2+}]_i$ with EGTA, change the $[Ca^{2+}]_i$ with the use of a microchamber, measure the open and shut interval durations with automated half-amplitude threshold analysis, bin and display log–log plots of interval dwell times, and fit dwell-time distributions with sums of exponentials are identical to those described in McManus & Magleby (1988). The precautions (including visual monitoring) used to prevent potential artifacts that can be associated with automated threshold analysis (Colquhoun, 1988) are detailed in McManus & Magleby (1989).

The effective cut-off frequency (−3 dB) for the filtering of the single-channel current record by the combined effects of the patch clamp, tape-recorder and final filter was typically 6–8 kHz (24 dB per octave). Effective filtering can be expressed in terms of dead time, which is the duration of a rectangular pulse which, when filtered, reaches 50% of its true amplitude (Colquhoun & Sigworth, 1983). The dead times for the analysis of channels 1–5 presented in this paper were: 36, 28·6, 60, 30·6 and 24·6 μs, respectively. The filtering was set so that noise peaks in the absence of channel activity would not be expected to exceed the half-amplitude level for threshold detection (see McManus & Magleby, 1988). Thus, the fast exponential components reflect channel activity and not noise.

Effective sampling periods of 5–15 μs were used to analyse the current records in order to reduce sampling promotion errors to negligible levels (McManus, Blatz & Magleby, 1987).

Estimating most likely rate constants with corrections for missed events

Figure 1 summarizes the iterative process used to estimate rate constants and calculate likelihoods for the examined kinetic schemes. Specific details for the individual steps in this

maximum likelihood fitting procedure may be found in Blatz & Magleby (1986*a*). (1) The first step is to calculate effective rate constants, based on the given kinetic scheme and dead time, to provide an approximate correction for the missed events which result from filtering. (2) The predicted distributions that would be observed with filtering are then calculated with the Q-matrix method

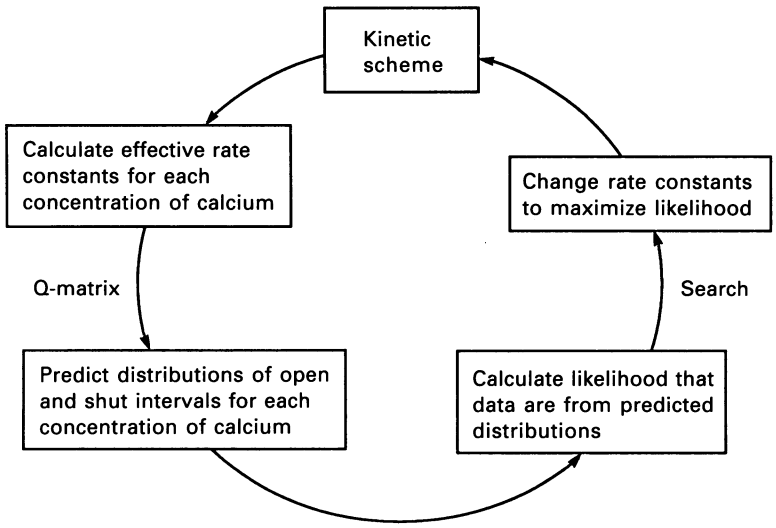

Fig. 1. Iterative method used to estimate the most likely rate constants for a given kinetic scheme. The use of effective rate constants corrects for missed events due to filtering. Dwell-time distributions obtained at three to four different $[Ca^{2+}]_i$ are simultaneously fitted with each pass around the loop to define better the rate constants and kinetic schemes. Further details in text.

(Colquhoun & Hawkes, 1977, 1981) using the effective rate constants. (3) The likelihood that the experimental data are drawn from the predicted distributions is then calculated from the experimental intervals and predicted distributions, using maximum likelihood methods, as described in Colquhoun & Sigworth (1983). (4) The estimated true rate constants are then changed using a maximization routine (see, for example, *Pattern Search* in Colquhoun (1971)), and steps (1)–(4) repeated until the most likely rate constants for the given kinetic scheme, dead time and experimental data are obtained. During the search, the rate constants are changed in a manner to preserve microscopic reversibility (Colquhoun & Hawkes, 1982, 1983) in order to be consistent with experimental observations (McManus & Magleby, 1989). Thus, when kinetic states are connected into loops, the value of one of the rate constants in each loop is determined by the other rate constants in the loops, such that the product of the rate constants in one direction around the loop equals the product of the rate constants in the other direction.

The correction for missed events used in the above analysis assumes that there is no noise in the experimental record and that the filtering is idealized, so that all events less than the dead time go undetected. Depending on the model and level of filtering, such assumptions can lead to errors which range from negligible to very large (McManus *et al.* 1987; Magleby & Weiss, 1990*a*). For the kinetic schemes and levels of filtering used in this paper, simulation showed (see Results) that these assumptions would typically lead to errors in estimates of the rate constants of about 1–12%.

Simultaneous fitting of dwell-time distributions obtained at several different $[Ca^{2+}]_i$

To increase the ability to identify kinetic schemes and rate constants, the search for the most likely rate constants, as illustrated in Fig. 1, was usually carried out with simultaneous fitting of dwell-time distributions obtained at three to four different $[Ca^{2+}]_i$ for each of the five single-channel patches. Thus, the calculation of the effective rate constants, the predicted distributions of open and shut intervals, and the likelihood calculation were performed (effectively) simultaneously for

three to four different $[Ca^{2+}]_i$ for each iterative pass around the loop in Fig. 1. This was done as follows. For the given kinetic scheme and rate constants the effective values of the Ca^{2+}-dependent rate constants for each $[Ca^{2+}]_i$ were determined by multiplying the Ca^{2+}-dependent rate constants (with units of $\mu M^{-1}\ s^{-1}$) by the $[Ca^{2+}]_i$. These and the non-Ca^{2+}-dependent rates were then used to determine effective rate constants for each $[Ca^{2+}]_i$. The predicted distributions for each $[Ca^{2+}]_i$ were then calculated with the Q-matrix method using the effective rate constants. The log-likelihood estimate for the simultaneous fitting of the experimental distributions obtained at the three to four different $[Ca^{2+}]_i$ was then the sum of the log-likelihood estimates for the distributions at each $[Ca^{2+}]_i$. Note that no weighting factors are used in calculating the log likelihood for the simultaneously fitted data; the maximum likelihood estimate for the simultaneously fitted data is the sum of the log-likelihood estimates for each individual interval at each $[Ca^{2+}]_i$.

Calculations

The fitting was performed in FORTRAN 77 on DEC 11/73 computer systems and also on XP accelerator boards (Cheshire Engineering Corp., Pasadena, CA, USA) inserted into the DEC machines. The accelerator boards decreased the computing time required for fitting by 4- to 5-fold. Without the accelerator board, fits for eight- to ten-state models took about 1–2 weeks. About 15–100 different kinetic schemes were fitted to data from each of the five channels. In addition, many of the kinetic schemes were typically refitted many times with different starting parameters to increase the probability that the most likely rate constants were found. The total computing time for this study exceeded the equivalent of seven years of DEC 11/73 computing time.

Estimating the theoretical best description of the data

In order to evaluate models it is useful to know the theoretical best description of the dwell-time distributions. This description can then be compared to the best description generated by any given kinetic scheme in order to evaluate how well the kinetic scheme describes the data. The theoretical best description of the dwell-time distributions has been estimated by fitting the dwell-time distributions with sums of exponentials, without any constraints on the areas and time constants of the exponential components, except that the areas must sum to 1·0 (Blatz & Magleby, 1986*b*). Thus, the areas and time constants are free parameters for the theoretical best description. In determining the theoretical best description, the number of fitted exponential components is increased until there is no further improvement in the maximum likelihood estimate. The likelihood estimate for the theoretical best description of the simultaneous fitting of dwell-time distributions obtained at several different $[Ca^{2+}]_i$ was obtained from the product of the maximum likelihood estimates for separate fittings of each individual distribution, or equivalently, the log-likelihood estimate was obtained from the sums of the log-likelihood estimates for each distribution.

Evaluating and ranking kinetic schemes

A normalized likelihood ratio (NLR) has been used to compare the ability of any given kinetic scheme to describe the experimental observations to the description given by the theoretical best fit. Normalization corrects for the difference in numbers of analysed intervals among experiments. The normalized likelihood ratio per 1000 intervals is defined as

$$\mathrm{NLR} = (S/T)^{(1000/N)}, \tag{1}$$

where S is the likelihood estimate for the experimental data given the kinetic scheme, obtained as described in Fig. 1, T is the likelihood estimate for the experimental data given the theoretical best description of the data, obtained as described in the previous section, and N is the total number of fitted intervals in the fitted dwell-time distributions. Note that the maximum likelihood estimates of S and T for the NLR are obtained by fitting the exact same data in two different ways. The normalized likelihood ratio is normalized to 1000 intervals, as this value is convenient for expression of the results. A value of 1·0 for the NLR would indicate that the given kinetic scheme describes the data as well as the theoretical best description. The likelihood ratio per single event can be calculated from the NLR values per 1000 events given in the paper from $\mathrm{NLR}^{(0.001)}$.

Since likelihoods are generally calculated as log likelihoods, the normalized likelihood ratio is calculated from

$$\mathrm{NLR} = \exp((\ln S - \ln T)/(N/1000)), \tag{2}$$

where ln is a natural logarithm. The normalized likelihood ratios then give a measure of how well different kinetic schemes describe the data, but they cannot be used directly for ranking schemes, since no penalty is applied for the number of free parameters.

To overcome this difficulty, the Schwarz criterion has been used to apply penalties and rank models (Schwarz, 1978; Ball & Sansom, 1989). The Schwarz criterion (SC) is given by

$$SC = -L + (0{\cdot}5F)(\ln N), \quad (3)$$

where L is the natural logarithm of the maximum likelihood estimate, F is the number of free parameters, and N is the number of intervals. The scheme with the smallest SC is then ranked first, and the scheme with the largest SC is ranked last.

Experimental and predicted plots of adjacent interval durations

Plots of the durations of open intervals adjacent to shut intervals of specified durations were generated as follows. Briefly, files containing the durations of sequential open and shut intervals during normal activity were scanned, and the open intervals were separated into groups based on the duration of the adjacent shut intervals. Open intervals occurring immediately before and immediately after the shut intervals of specified durations were tabulated together, since their means were not significantly different (McManus & Magleby, 1989). The plotted point for a given specified range was then located by the mean of all the shut intervals that fell into the specified range and the mean of the open intervals adjacent to the shut intervals in the specified range. The ranges of shut intervals were overlapping to increase the numbers of intervals in each range. For example, the first five specified ranges of shut intervals for channel 1 in Fig. 7*A* for 21·6 μM $[Ca^{2+}]_i$ were (ms): 0–0·056; 0·032–0·097; 0·056–0·17; 0·097–0·29; 0·17–0·5.

A similar procedure was used to generate adjacent interval plots of shut intervals adjacent to open intervals of specified durations, but with the open and shut intervals reversed from that described above.

The predicted adjacent interval plots were calculated by first simulating 500000 detected intervals for the given kinetic scheme and level of filtering used in the experiment, as described in Blatz & Magleby (1986*a*). Filtering was performed by assuming idealized filtering, such that intervals with true durations less than the dead time go undetected, with the duration of the missed intervals being combined with the durations of the preceding and following intervals. For example, with a dead time of 0·03 ms and observed intervals of 0·4, 0·5, 0·02, 0·01, 0·2, and 1 ms, the durations of the filtered intervals with idealized filtering would be 0·4, 0·73, and 1 ms. The predicted adjacent interval plots were then obtained by analysing the files of sequential simulated intervals in the exact same manner used to analyse the files of sequential experimental intervals.

Estimating errors with resampling

Resampling methods (Efron, 1982; Horn, 1987) were used to obtain estimates of errors associated with determining areas and time constants of exponential components fitted to dwell-time distributions, as in Fig. 5. For each experimental dwell-time distribution, five different artificial dwell-time distributions were created by drawing intervals at random from the experimental distribution. Drawing was done with replacement so that some experimental intervals could be used several times and some not at all. Each artificial distribution was then fitted with sums of exponentials using maximum likelihood techniques, as was done for the experimental distribution. The standard deviations of the estimates of the areas and time constants for the fitting of the artificial distributions then gives an estimate of the uncertainty in the parameters fitted to the experimental distributions.

Resampling was also used to estimate errors in rate constants associated with the simultaneous fitting of dwell-time distributions, as in Table 1. The dwell-time distributions obtained at the different $[Ca^{2+}]_i$ for a given channel were resampled with replacement to obtain artificial distributions, which were then simultaneously fitted to obtain rate constants from the resampled distributions. This entire procedure was repeated five times for the given channel to obtain the standard deviations of the estimated rate constants.

Once the standard deviations were obtained for each rate constant it was possible to calculate whether the estimated rate constants for different channels were different. This was done by calculating the overlapping areas of the distributions of rate constants defined by their standard deviations (Horn, 1987). If the overlapping area was less than 5%, then the compared parameters were considered to be significantly different ($P < 0{\cdot}05$).

RESULTS

Currents through a large-conductance Ca^{2+}-activated K^+ channel (BK or maxi K^+ channel) are shown in Fig. 2 for three different concentrations of Ca^{2+} at the inner membrane surface, $[Ca^{2+}]_i$. The excised patch of membrane, which contained a single

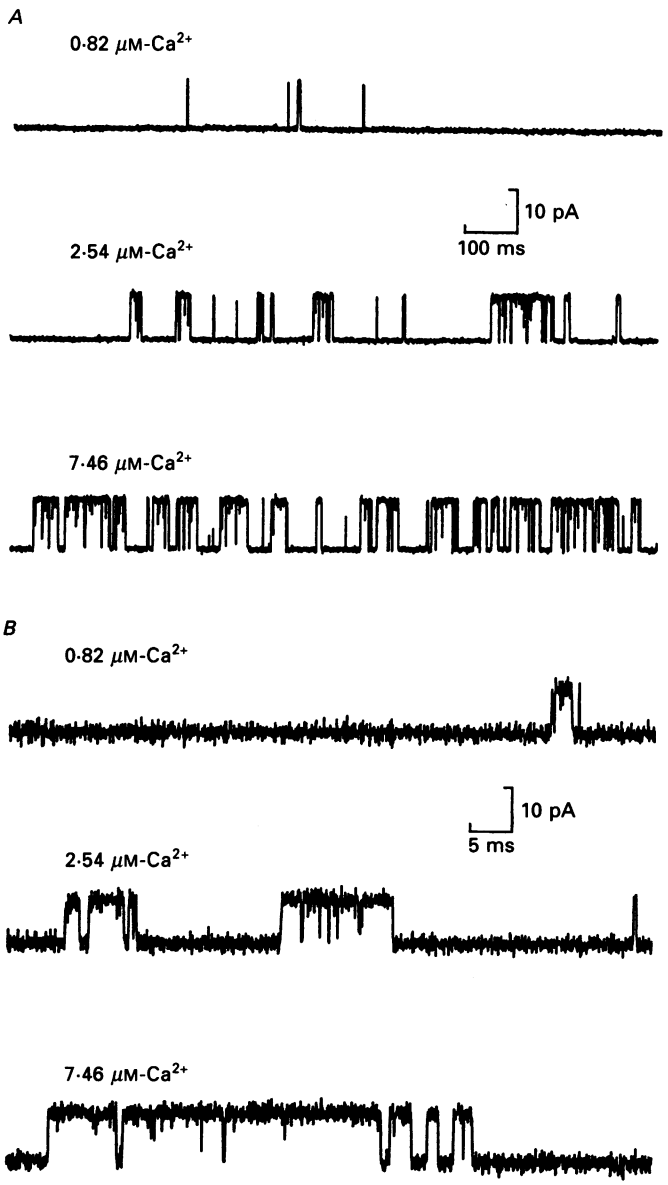

Fig. 2. Single-channel currents recorded from a large-conductance Ca^{2+}-activated K^+ channel at three different concentrations of $[Ca^{2+}]_i$. Upward current steps indicate channel opening. A microchamber (Barrett *et al.* 1982) was used to change the solution. Data are presented at a slow time base in *A* and at a faster time base in *B*. The effective low-pass filtering was 1·24 kHz in *A* (for illustration) and 6·44 kHz in *B* (−3 dB, 24 dB per octave). Data for this figure and the rest of the paper were obtained at a membrane potential of +30 mV. Channel 2.

channel, was held at +30 mV, the voltage used for all the experiments reported in this paper. Records are shown at a slow time base in *A* and at a faster time base in *B*, as $[Ca^{2+}]_i$ was increased from 0·82 to 7·45 μM. The increase in P_{open} with increasing $[Ca^{2+}]_i$ is characteristic of maxi K^+ channels (Marty, 1981; Barrett *et al.* 1982; Latorre, Vergara & Hidalgo, 1982; Wong, Lecar & Adler, 1982), and results from complex changes in channel kinetics (Methfessel & Boheim, 1982; Magleby & Pallotta, 1983*a*, *b*; Moczydlowski & Latorre, 1983). The objective of this paper is to explain these Ca^{2+}-induced changes in activity.

Estimating the minimum number of bound Ca^{2+} from Hill plots

An estimate of the minimum number of bound Ca^{2+} required to fully activate the maxi K^+ channel can be obtained from the slope of Hill plots, where $P_{open}/(1-P_{open})$ is plotted against $[Ca^{2+}]_i$ on double logarithmic co-ordinates, or equivalently, from the Hill coefficient obtained by fitting the Hill equation to experimental data that has not been transformed (e.g. Colquhoun, 1973). The relationship between $[Ca^{2+}]_i$ and P_{open} for three single channels is plotted in Fig. 3*A–C*, where the continuous lines plot the fits to the data with the Hill equation (see legend for details). The slopes (Hill coefficients) were 3·1, 2·2 and 4·2, and the $[Ca^{2+}]_i$ for a P_{open} of 0·5 ($K_{0.5}$) was 21, 5·9 and 8·1 μM, in Fig. 3*A–C*, respectively. There was considerable variability among the different channels in both the Hill coefficients and in the value of $K_{0.5}$. This is emphasized in Fig. 3*D*, which plots P_{open} against $[Ca^{2+}]_i$ for channels in thirteen different excised patches. Data obtained at a pH of 7·2 are plotted with dashed lines and data obtained at a pH of 7·0 are plotted with continuous lines. A wide variation in slope and 4- to 5-fold range in $K_{0.5}$ at each pH for the different channels is apparent, consistent with previous observations of variability in $[Ca^{2+}]_i$ sensitivity among maxi K^+ channels (Moczydlowski & Latorre, 1983; Singer & Walsh, 1987). Similar to this variability, cloned receptors for acetylcholine receptor channels also do not produce homogeneous behaviour (Gibb, Kojima, Carr & Colquhoun, 1990).

Although different channels could have differences in P_{open} for a given $[Ca^{2+}]_i$, consecutive estimates of P_{open} for a given channel for a fixed $[Ca^{2+}]_i$ were usually relatively stable. However, some of the channels (about 15%) showed unstable variations in gating for a fixed $[Ca^{2+}]_i$ that were characterized by slow changes in P_{open} and in the mean open and mean closed times. Channels showing this behaviour were not analysed further.

For the data obtained at a pH of 7·0 in Fig. 3 the mean Hill coefficient was $3·7 \pm 0·8$ (range 3·0–5·0), and $K_{0.5}$ was $13·6 \pm 7·0$ μM (six patches). At a pH of 7·2 the mean Hill coefficient was $3·0 \pm 0·5$ (range 2·2–3·7), and $K_{0.5}$ was $9·2 \pm 6·1$ μM (seven patches; an eighth patch with pronounced inactivation and a slope of 1·3 was excluded). Mean Hill coefficients from three to four suggest that a minimum of three to four Ca^{2+} typically bind to fully activate the channel under the conditions of our experiments (with no added Mg^{2+}). Hill slopes greater than four were observed in two of thirteen experiments, with values of 4·1 and 5·0, suggesting that a minimum of five Ca^{2+} bindings may be required to fully activate the channel in some cases.

When data from each patch were analysed separately and then compared, the effect of pH on the shift in $K_{0.5}$ was not significant ($0·05 < P < 0·1$), due to the large variability among channels. When the data from all the experiments at each

pH were averaged before fitting, the shift in $K_{0.5}$ was significant ($P < 0.05$). A decrease in $K_{0.5}$ with increased pH is consistent with the effect of pH on maxi K^+ channels from other tissues (Cook, Ikeuchi & Fujimoto, 1984; Christensen & Zeuthen, 1987; Blatz, 1989; Kume, Takagi, Satake, Tokuno & Tomita, 1990;

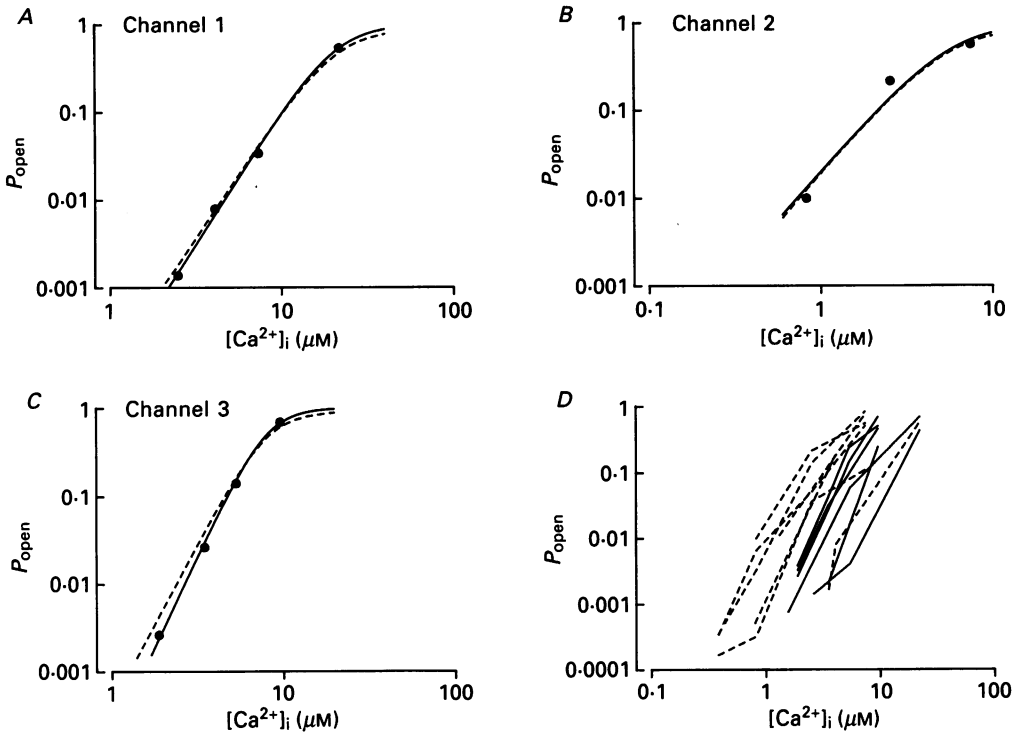

Fig. 3. Plots of P_{open} *versus* $[Ca^{2+}]_i$ on double logarithmic co-ordinates. *A–C*, data for channels 1–3; ●, experimental observations. Estimates of n, the Hill coefficient, and $K_{0.5}$, the $[Ca^{2+}]_i$ for a P_{open} of 0·5, were obtained by least-squares fitting of the data with the equation: $\log (P_{open}/(1-P_{open})) = n(\log Ca^{2+}) + C$, where $K_{0.5} = (10^{-C})^{1/n}$. The values of n and $K_{0.5}$ are in Table 1. The continuous lines plot the least-squares fits to the data, calculated with: $P_{open} = (Ca^{2+})^n/(10^{-C} + (Ca^{2+})^n)$. The dashed lines plot the predicted P_{open} for scheme X using the rate constants in Table 1. *D*, individual plots of P_{open} *versus* $[Ca^{2+}]_i$ for data from seven excised patches at pH 7·2 (dashed lines) and for data from six excised patches at pH 7·0 (continuous lines). The lines in *D* connect the experimental observations.

Laurido, Wolff & Latorre, 1990). The apparent increased Hill coefficient at reduced pH was not significant by either method of analysis ($P > 0.2$).

The Hill slopes observed in the present study at pH 7·2 and without Mg^{2+} in the solutions are similar to those of 2·8 and 2·9 observed at pH 7·2 in previous experiments on maxi K^+ channels from cultured rat muscle with 2 mM-Mg^{2+} in the solutions (Barrett *et al.* 1982; Magleby & Pallotta, 1983*b*). In comparison, the Hill coefficients for maxi K^+ channels from adult skeletal muscle inserted in lipid bilayers is only about two when the solutions do not contain Mg^{2+} (at pH of 7·2), and ranges from 3·2 to 5·4 with a mean of 4·2 for solutions with 10 mM-Mg^{2+} (Golowasch, Kirkwood & Miller, 1986; Oberhauser, Alvarez & Latorre, 1988).

Analysis of five different single-channel patches during normal activity

The results presented in the rest of the paper are based on the analysis of five different patches containing a single maxi K^+ channel. The analysis is restricted to activity during the normal mode, which includes about 96% of the intervals, and is easily identified with stability plots (McManus & Magleby, 1988). The stability plots also indicated that the activity during the normal mode for the five analysed channels were reasonably stable. About 200000 intervals during normal mode activity (range 92000–308000) were analysed for each of the five channels. Data from individual channels were always analysed separately because different channels can have different properties, as shown in Fig. 3.

Ca^{2+} shifts the open and shut dwell-time distributions

Figure 4 presents dwell-time distributions obtained from a single channel at three different $[Ca^{2+}]_i$. The circles plot the experimental observations and the continuous lines plot the maximum likelihood fits (Colquhoun & Sigworth, 1983; McManus & Magleby, 1988) with the sums of three exponentials for the open distributions and five exponentials for the shut. The dashed lines plot the individual exponential components. The distributions at the different $[Ca^{2+}]_i$ have been scaled to contain the same number of events so that direct comparisons can be made. Increasing $[Ca^{2+}]_i$ shifted the open intervals from briefer to longer durations (*Aa–Ca*), and shifted the shut intervals from the longer to briefer durations (*Ab–Cb*), as expected from the effects of $[Ca^{2+}]_i$ on the single-channel currents in Fig. 2.

Figure 5 details these shifts by plotting the time constants and areas of the fitted exponential components as a function of $[Ca^{2+}]_i$. The components are numbered in terms of their time constants, from fastest to slowest, with component 1 being the fastest. Increasing $[Ca^{2+}]_i$ increased the time constants of the two slower open components (Fig. 5*A*) and shifted area from the two faster open components to the slowest open component (Fig. 5*B*). For the channel presented in Fig. 5 the open distributions were best described by the sums of three exponentials. However, about 30% of the open distributions for maxi K^+ channels are best described by four exponential components (McManus & Magleby, 1988). For those channels in which the data were best described by four components, an additional component with a time constant between those of components 2 and 3 was usually observed. The time constant of this component typically increased with $[Ca^{2+}]_i$ and its area decreased.

Increasing $[Ca^{2+}]_i$ also decreased the time constants of the two (or possibly three) slowest shut components (Fig. 5*C*) and shifted area from the slowest shut component to the next slowest (Fig. 5*E*) and to the three fastest components (Fig. 5*D*). The second slowest shut component first increased in area and then decreased as $[Ca^{2+}]_i$ was increased (Fig. 5*E*).

Five shut components were initially fitted to the data for Figs 4 and 5 in order to explore the simplest models that might account for the major features of the data (see following sections and Discussion). However, the shut distributions were often best described with six to eight significant exponential components (McManus & Magleby, 1988). One or more of these additional components was typically a long-lasting (inactive) shut state that was entered so infrequently (zero to several times every 10000 events) that intervals from this component had little effect on the

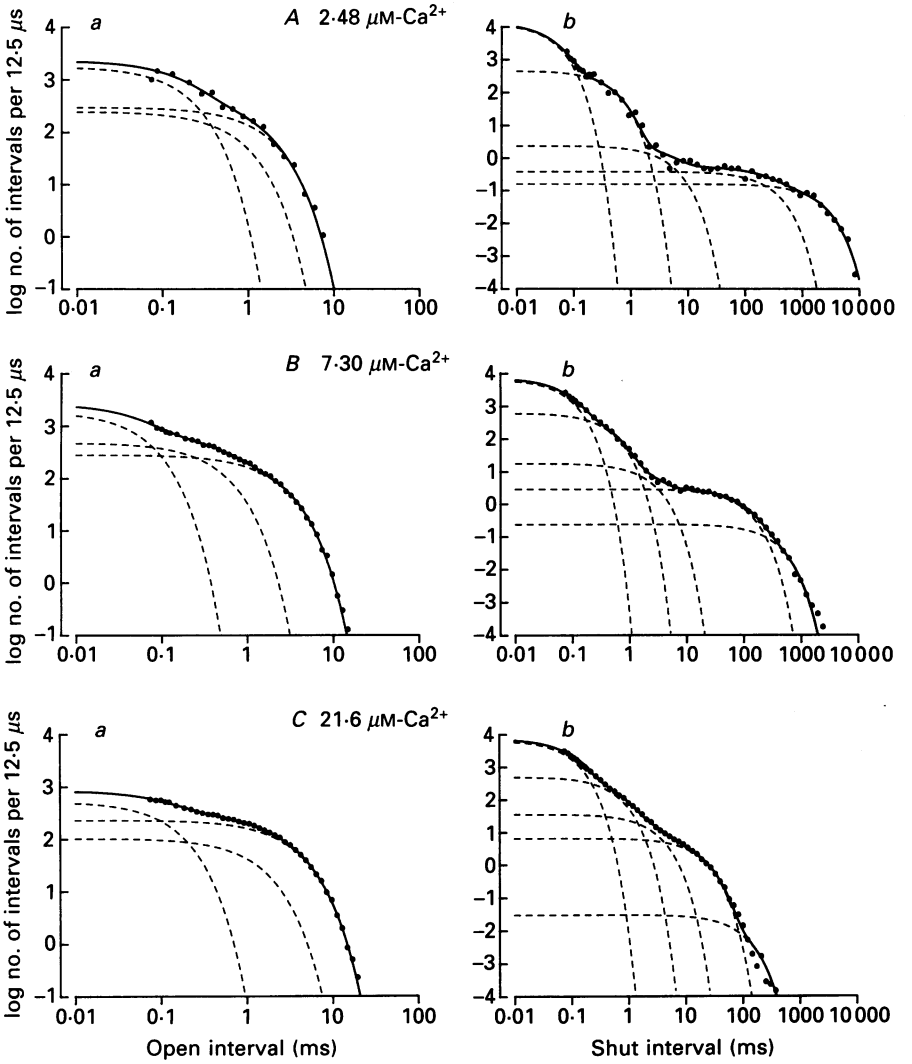

Fig. 4. Ca^{2+}-dependence of dwell-time distributions. ●, numbers of observed open (*a*) and shut (*b*) intervals plotted against their durations on double logarithmic co-ordinates for data obtained at three different $[Ca^{2+}]_i$ (*A–C*). The continuous lines are the maximum likelihood fits with the sums of three exponential components to the open distributions and the sums of five exponential components to the shut distributions. The individual components are indicated by the dashed lines. The number of fitted events (those with durations greater than twice the dead time of 36 μs) were, for the open and shut distributions: 2·48 μM $[Ca^{2+}]_i$, 871 and 798; 7·30 μM $[Ca^{2+}]_i$, 17489 and 14773; 21·6 μM $[Ca^{2+}]_i$, 57678 and 44142. The ordinate applies directly to the distributions obtained at 21·6 μM $[Ca^{2+}]_i$. In order to allow direct comparisons of the distributions obtained at the different $[Ca^{2+}]_i$, the other distributions were scaled to contain the same number of events, estimated from 0 ms to infinity, as the distributions at 21·6 μM $[Ca^{2+}]_i$. The estimated number of events in each distribution was calculated from the fitted number (those events with durations greater than twice the dead time) divided by the fraction of events in the predicted distributions with durations greater than twice the dead time. The multiplying factors for the open and shut distributions were: 2·48 μM $[Ca^{2+}]_i$, 58·6 and 49·9; 7·30 μM $[Ca^{2+}]_i$, 2·98 and 3·13. Channel 1.

results when fitting with seven or fewer components. The basis for the long-lasting shut state is not known, but it may represent infrequent Ca^{2+} (or contaminating Ba^{2+}) block of the channel (Vergara & Latorre, 1983). The one to two additional components that are observed when fitting with six or more components typically

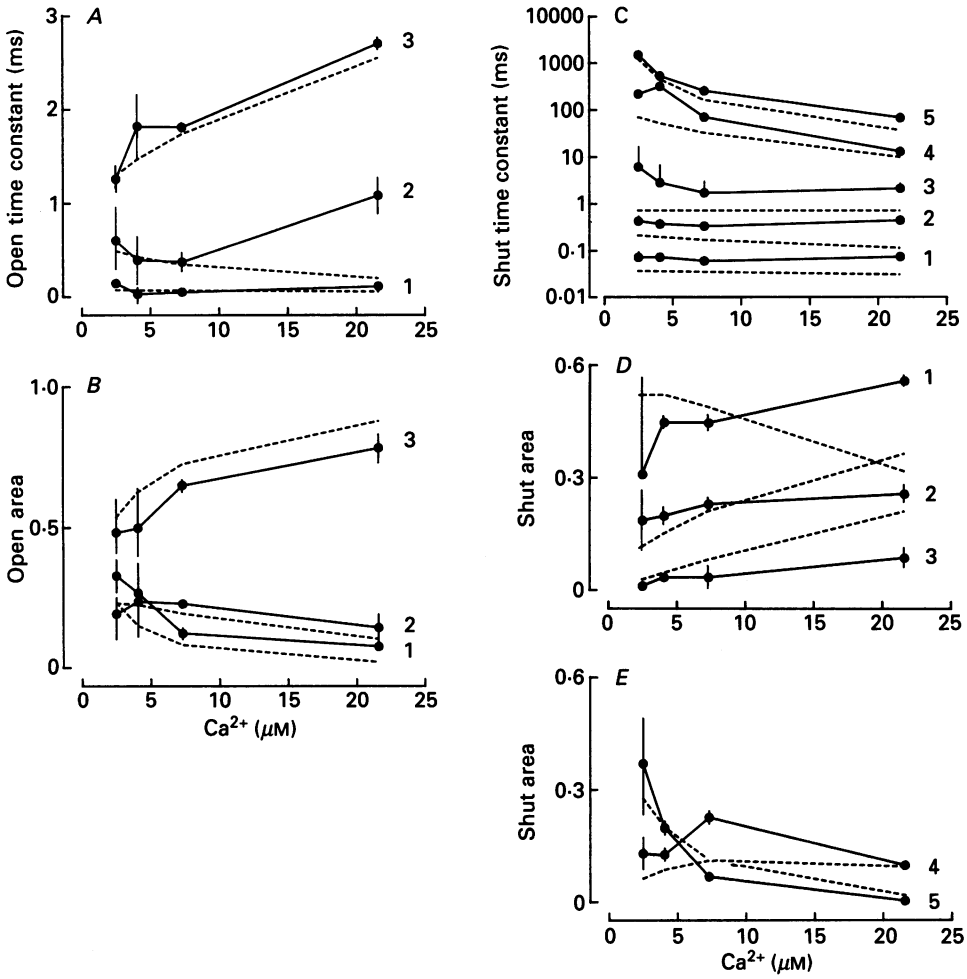

Fig. 5. Ca^{2+} dependence of the exponential components describing the dwell-time distributions in Fig. 4. *A* and *B*, the three exponential components describing the open distributions as a function of $[Ca^{2+}]_i$. *C*, *D* and *E*, the five exponential components describing the shut distributions as a function of $[Ca^{2+}]_i$. The components are numbered from fastest to slowest with component 1 being the fastest. The filled symbols and continuous lines plot the time constants and areas of the exponential components determined by fitting sums of exponentials to the distributions in Fig. 4. Because of the limited data at the lowest $[Ca^{2+}]_i$, the time constant of the fastest component of the shut distribution obtained in 2·48 μM-Ca^{2+} was fixed at 0·72 μs for the fitting. The likelihood value of the fit with the fixed time constant did not differ significantly from that with the time constant free. The bars indicate standard deviations estimated by resampling (see Methods), and in some cases are plotted in only one direction. The dashed lines plot the time constants and areas of the exponential components predicted by scheme X with the rate constants in Table 1. Channel 1.

had limited amounts of area and combined with one or more of the five components when fitting with only five exponentials. When the shut distributions were fitted with additional components, the general effects of increased $[Ca^{2+}]_i$ on the shut distributions were the same as when fitting with fewer components. The time constants of the two to three slower shut components (excluding the inactive shut component, which occurred too infrequently to study) decreased and area was shifted from the two to three slower components towards the faster components.

For all five channels the Ca^{2+}-dependent shifts in the open and shut dwell-time distributions were generally similar.

Requirements for the Ca^{2+}-activated gating mechanism for the maxi K^+ channel: a general model

The results in Figs 2–5 and those from previous studies suggest that the gating mechanism for normal mode activity of the maxi K^+ channel from skeletal muscle should have the following features.

(1) The channel should typically bind three to four or more Ca^{2+} ions for maximum activity, as indicated by Hill slopes of 2·2–5 (Figs 2 and 3; Barrett *et al.* 1982; Magleby & Pallotta, 1983*a*, *b*; Golowasch *et al.* 1986; Oberhauser *et al.* 1988).

(2) The channel should have at least three to four open states and six to eight closed states, as indicated by the number of exponential components in the dwell-time distributions (McManus & Magleby, 1988). If the infrequently entered long-lasting inactive closed state is excluded, then the channel would need a minimum of five closed states. Note that the binding of four Ca^{2+} requires at least five closed (C) states (C, C_{Ca}, C_{2Ca}, C_{3Ca}, C_{4Ca}).

(3) Both open and closed states should be capable of binding and unbinding Ca^{2+}, as indicated by the Ca^{2+}-dependent shifts in the time constants of both the open and closed exponential components (Fig. 5; Methfessel & Boheim, 1982; Magleby & Pallotta, 1983*a*; Moczydlowski & Latorre, 1983.

(4) The gating should appear consistent with a Markov process in which the transition rates from any given state depend only on the state that the channel is in and not on the history of the preceding transitions. Some support consistent with Markov gating comes from the observation that the time constants of the components in the dwell-time distributions are independent of previous channel activity (McManus & Magleby, 1989). Simple fractal models for the gating can be excluded (Korn & Horn, 1988; McManus, Weiss, Spivak, Blatz & Magleby, 1988).

(5) The channel should have two or more independent transition pathways between open and closed states to account for the dependent relationship between the durations of adjacent intervals (McManus, Blatz & Magleby, 1985; McManus & Magleby, 1989).

(6) The gating should be consistent with microscopic reversibility, as indicated by the observation that the relationship between the durations of adjacent open and closed intervals are independent of the time direction of analysis (McManus & Magleby, 1989).

(7) The longer duration open states (or effective compound open states) should, in general, be connected to the briefer duration closed states, and the briefer duration open states should, in general, be connected to the longer duration closed states. Such

connections among open and closed states could give rise to the observed inverse relationship in the durations of adjacent open and shut intervals (McManus & Magleby, 1989).

(8) Increasing $[Ca^{2+}]_i$ should drive the channel from the longer duration (effective and/or compound) closed states and briefer duration open states towards the briefer duration closed states and the longer duration open states, as indicated by the Ca^{2+}-dependent shifts in the components of the dwell-time distributions (Figs 4 and 5, Magleby & Pallotta, 1983*a*). Furthermore, openings to the longer duration open states should require more Ca^{2+} bindings than openings to the briefer duration open states, as indicated by the greater Ca^{2+} dependence of the frequency of openings to the longer openings when compared to briefer openings (Magleby & Pallotta, 1983*a*).

A general kinetic model consistent with all these observations is given by scheme I

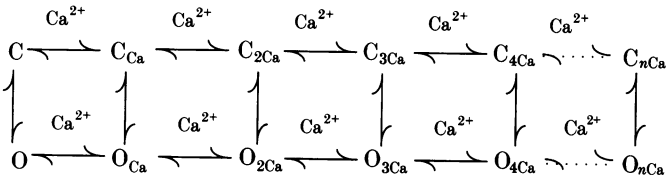

(I)

where C represents closed states, O represents open states, n is in the range of 3–6, and, in general, the effective lifetimes of the closed states decrease from left to right, and the effective lifetimes of the open states increase from left to right. Opening–closing transitions (vertical arrows) are separate from the binding and unbinding steps (horizontal arrows), since it is assumed that binding and opening (or unbinding and closing) do not occur simultaneously. For example, if binding initiates opening, then the binding must precede opening, resulting in separate binding and opening steps.

In agreement with the requirements for gating summarized above, scheme I has sufficient states to account for the observed components in the dwell-time distributions: it can bind sufficient internal Ca^{2+} to account for the observed Hill coefficients, both open and closed states bind Ca^{2+}, there are multiple transition pathways between open and closed states, the indicated trend in state lifetimes could give an inverse relationship between the durations of adjacent open and closed intervals, and increasing $[Ca^{2+}]_i$ would drive the channel towards the longer open and briefer closed states. In addition, scheme I will yield Markov gating if the rate constants do not change with time, and scheme I can be consistent with microscopic reversibility with appropriate rate constants.

Scheme I is an obvious extension of the model proposed by Magleby & Pallotta (1983*a*) for gating of the maxi K^+ channel, and appears similar to the Monod, Wyman & Changeux (1965) model for oxygen binding by haemoglobin. McManus *et al.* (1985) suggested that scheme I might account for the dependent relationship between adjacent interval durations, and variations of scheme I have proven useful to study the gating of the glutamate receptor channel (Kerry, Ramsey, Sansom & Usherwood, 1988; Bates, Sansom, Ball, Ramsey & Usherwood, 1990). The following sections of this paper examine whether gating mechanisms based on scheme I might account for the Ca^{2+} dependence of the maxi K^+ channel.

Some specific Ca^{2+}-dependent gating mechanisms

The general gating mechanism described by scheme I contains more open states than are detected in the experimental data. It is also not known how many Ca^{2+} bindings are required for any particular channel since the observed range of Hill coefficients from different channels can be quite large (2·2–5·0). It is also not known how many shut states are needed to capture the major features of the Ca^{2+}-dependent kinetics. Thus, within the general framework of scheme I, a number of specific gating mechanisms were created by eliminating various states and transition pathways. These models are:

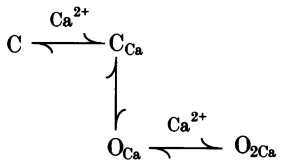

(II)

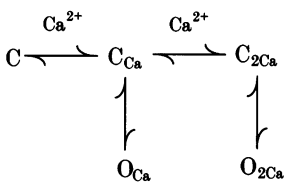

(III)

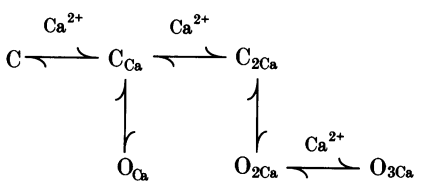

(IV)

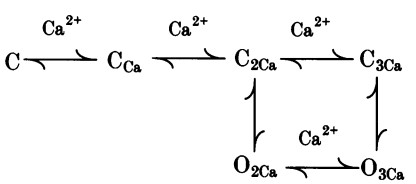

(V)

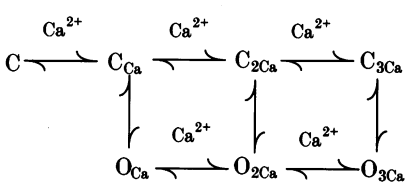

(VI)

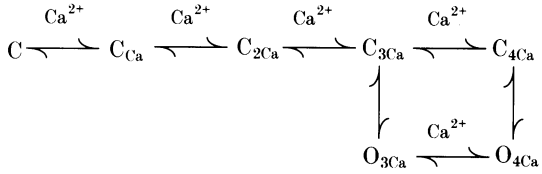

(VII)

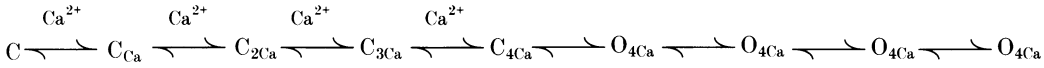

(VIII)

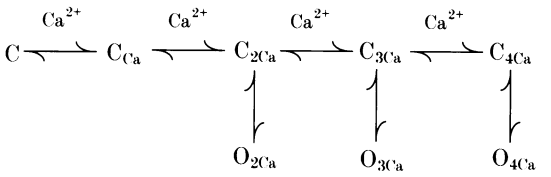

(IX)

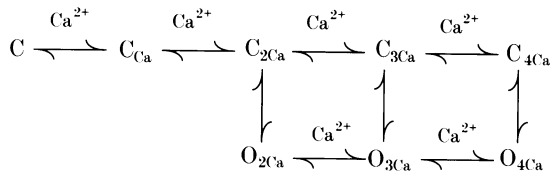

(X)

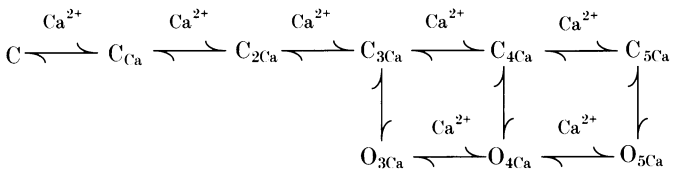

(XI)

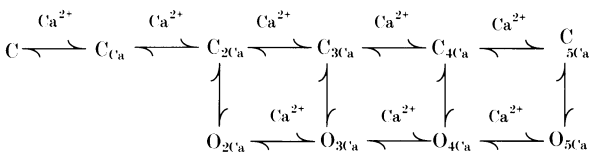

(XII)

Scheme II was used by Moczydlowski & Latorre (1983) and schemes III and IV were used by Magleby & Pallotta (1983*a*) to investigate the gating of maxi K^+ channels. Scheme III has also been widely used for the acetylcholine receptor channel (Colquhoun & Hawkes, 1977; Dionne, Steinbach & Stevens, 1978; Colquhoun & Sakmann, 1985; Fredkin *et al.* 1985) and can account for the correlations between openings for this channel (Jackson, Wong, Morris & Lecar, 1983).

Evaluation of schemes II–XII requires: (1) estimating the most likely rate constants for the transitions among the various states; (2) ranking the schemes in terms of the likelihood that the experimental data were generated by the schemes; and (3) determining if the highest ranked schemes can account for the major features of the Ca^{2+} dependence of the channel.

Most likely rate constants were estimated, as described by Fig. 1 in the Methods, by maximum likelihood fitting of dwell-time distributions using iterative Q-matrix calculations (Colquhoun & Hawkes, 1977, 1981). Effective rate constants were used to correct for missed events, as detailed in Blatz & Magleby, (1986*a*). Schemes were evaluated in two ways: by fitting dwell-time distributions obtained at a single $[Ca^{2+}]_i$, and by the simultaneous fitting of dwell-time distributions obtained at three or four different $[Ca^{2+}]_i$.

Dwell-time distributions obtained at a single $[Ca^{2+}]_i$ are usually insufficient to define a unique kinetic scheme or set of rate constants

As expected from theoretical (Fredkin *et al.* 1985; Bauer *et al.* 1987; Magleby & Weiss, 1990*b*) and experimental (Blatz & Magleby, 1986*b*; Weiss & Magleby, 1989) studies, there was usually insufficient information in the dwell-time distributions obtained at a single $[Ca^{2+}]_i$ to define unique models or rate constants. Consequently, several models and sets of rate constants for each model could usually be found that described the distributions obtained at the single $[Ca^{2+}]_i$ as well as theoretically possible (see Methods). Furthermore, the kinetic schemes and rate constants that could describe the dwell-time distributions obtained at a single $[Ca^{2+}]_i$ could not then adequately describe the Ca^{2+}-dependent shifts in the dwell-time distributions. The observation that dwell-time distributions obtained under a single set of experimental conditions are not necessarily sufficient to uniquely define gating mechanism will not be described in detail since similar findings have been presented previously (Magleby & Pallotta, 1983*a*; Blatz & Magleby, 1986*b*).

Simultaneous fitting of dwell-time distributions obtained at different $[Ca^{2+}]_i$

Fitting dwell-time distributions obtained at a single $[Ca^{2+}]_i$ was not sufficient to define schemes III–XII and the rate constants for these schemes because there was insufficient kinetic information in the dwell-time distributions obtained at a single $[Ca^{2+}]_i$. For example, a measure of the kinetic information G in the dwell-time distributions generated by a Markov model with n open and m shut states is give by

$$G = (2n-1)+(2m-1), \tag{3}$$

where n open and m shut exponential components sum to generate the open and shut distributions. For a model with three open states, as in scheme X, the open dwell-time distribution would be described by the sum of three exponentials, each with an area and time constant. Since the areas must sum to 1·0, one of the three areas is fixed by the other two. Hence, the maximum number of parameters that could be obtained from the open distribution would be five $(2\times3-1)$. A similar calculation indicates that a maximum of nine parameters $(2\times5-1)$ could be derived from the shut distribution form scheme X.

Thus, for an eight-state model, the open and shut dwell-time distributions obtained at a single $[Ca^{2+}]_i$ could yield up to fourteen separate experimentally determined parameters, provided that all the components could be detected. As indicated in the previous section, this was insufficient information to uniquely determine the sixteen free parameters required to define the rate constants for scheme X, or even to determine the fourteen parameters required to define the rate constants for scheme IX. Decreasing the numbers of states in a model does not

necessarily increase the ability to define models and rate constants because the predicted number of exponential components, and hence the kinetic information content when fitting, decreases with the number of states in the fitted model.

What is needed, then, is a means to obtain additional kinetic information about the gating without increasing the number of free parameters. Simultaneous fitting of dwell-time distributions obtained at three to four different $[Ca^{2+}]_i$ may provide such a method (McManus & Magleby, 1986; Bauer *et al.* 1987; Ball & Sansom, 1989; Kienker, 1989; Balser, Roden & Bennett, 1990; and see precautions in Goldman, 1991). This is the case since the number of free parameters for any given model remains the same with simultaneous fitting, while the dwell-time distributions obtained at each additional $[Ca^{2+}]_i$ can provide additional kinetic information because of their Ca^{2+} dependence (Figs 4 and 5). However, the kinetic information is not likely to increase in direct proportion to the number of experimental conditions included in the simultaneous fitting because many of the rate constants are expected to be independent of $[Ca^{2+}]_i$, and the apparent new information obtained for each new $[Ca^{2+}]_i$ may not be independent of previous information. Thus, while simultaneous fitting should increase the ability to determine models and rate constants, there will still be some models and rates constants that are poorly defined or undefinable with simultaneous fitting.

Simultaneous fitting can increase the ability to define kinetic schemes and rate constants

Estimates of the most likely rate constants for schemes II–XII were determined by simultaneously fitting dwell-time distributions obtained at three to four different $[Ca^{2+}]_i$ for each of the five different single maxi K^+ channels. Data obtained from each channel were analysed separately. For schemes II–VII, IX and X an apparent single most likely set of rate constants was found for each scheme and channel with simultaneous fitting, in contrast to the multiple solutions that were found when fitting distributions obtained at a single $[Ca^{2+}]_i$. For these schemes, estimates of the most likely rate constants for any given channel and model were typically reproducable within about 1% for repeated simultaneous fitting with different starting parameters. While this observation is consistent with one best solution for each of these schemes, it does not establish that the most likely rate constants are defined within such a narrow range. This can be seen in Table 1 which presents the most likely rate constants for scheme X for each of the five channels, together with estimates of the standard deviations for channels 1 and 2, as determined with resampling (Efron, 1982; Horn, 1987; see Methods). Schemes XI and XII also appeared to have single most likely solutions with simultaneous fitting, but because of the complexity of these schemes and the fitting time required for each solution, fewer fittings were performed.

The observation of an apparent single most likely solution for a kinetic scheme does not exclude the possibility that additional equally likely solutions or even more likely solutions might be found with additional fitting. The chance of having found the most likely solution for the various schemes is greatest for scheme II and least for scheme XII, since the difficulty in finding the most likely solution increases with the numbers of states and loops in a model.

TABLE 1. Estimated rate constants for scheme X

	Channel				
	1	2	3	4	5
pH	7·2	7·2	7·0	7·0	7·0
Hill coefficient	3·1	2·2	4·2	3·0	3·0
$K_{0.5}$ (μM)	20·9	5·87	8·10	16·0	26·7
Rate units					
1, 2 s^{-1}	1090 ± 28	1970 ± 45	602	1760	1932
1, 4 s^{-1}	181 ± 2·6	< 0·1 ± < 0·1	149	131	149
2, 1 μM^{-1} s^{-1}	142 ± 6·2	117 ± 6·0	280	184	220
2, 3 s^{-1}	15·4 ± 5·1	71·6 ± 9·1	38·3	33·9	46·2
2, 5 s^{-1}	2090 ± 78	745 ± 8·2	4890	1570	2600
3, 2 μM^{-1} s^{-1}	214 ± 61	874 ± 122	1563	431	630
3, 6 s^{-1}	13900 ± 1220	2730 ± 172	8920	8820	19000
4, 1 s^{-1}	1390 ± 42	< 0·1 ± < 0·1	1600	1017	732
4, 5 s^{-1}	< 0·1 ± < 0·1	1060 ± 30	< 0·1	< 0·1	< 0·1
5, 2 s^{-1}	19100 ± 1060	16700 ± 456	24800	21000	18900
5, 4 μM^{-1} s^{-1}	< 0·1 ± < 0·1	338 ± 14	< 0·1	< 0·1	< 0·1
5, 6 s^{-1}	9850 ± 618	4440 ± 84	6120	6120	6180
6, 3 s^{-1}	426 ± 49	507 ± 35	169	493	321
6, 5 μM^{-1} s^{-1}	459 ± 28	448 ± 20	932	326	196
6, 7 s^{-1}	3800 ± 123	1420 ± 64	3010	1850	2270
7, 6 μM^{-1} s^{-1}	6·53 ± 0·36	15·3 ± 0·18	12·5	7·38	8·35
7, 8 s^{-1}	8·23 ± 2·9	1·87 ± 0·27	4·10	4·54	8·79
8, 7 μM^{-1} s^{-1}	1·41 ± 0·26	4·44 ± 0·26	1·09	0·504	0·459

Estimates of the standard deviations for channels 1 and 2 were determined by fitting resampled dwell-time distributions. The numbering of the states for scheme X is indicated below. All of the forward (left to right) steps involve the binding of a Ca^{2+} ion. These binding steps are indicated in the above table with the units of μM^{-1} s^{-1}. The Ca^{2+}-dependent rate constants can be expressed with units of M^{-1} s^{-1} by multiplying by 10^6.

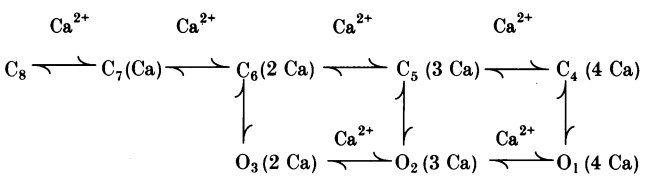

(X)

In contrast to the other schemes, two equally likely solutions were found with simultaneous fitting for scheme VIII (there may be more), presumably because the connected (compound) open states with rate constants independent of $[Ca^{2+}]_i$ and the single transition pathway between open and shut states place fewer restrictions on the rate constants.

Evaluating and ranking the various schemes

Normalized likelihood ratios were used to evaluate the ability of the various kinetic schemes to describe the distributions. The normalized likelihood ratio for a given kinetic scheme is the ratio of the probability (density) that the experimental data are drawn from the distributions predicted by that kinetic scheme to the probability (density) that the experimental data are drawn from the distributions given by the theoretical best description of the experimental data per 1000 events

(eqns (1) and (2) in Methods). A normalized likelihood ratio of 1·0 indicates that a kinetic scheme describes the distributions as well as theoretically possible. A normalized likelihood ratio of 0·01 indicates that the probability (density) that the experimental data were drawn from the distributions predicted by the given kinetic

TABLE 2. Normalized likelihood ratios (NLR) and rankings (R) of schemes II–XII

	Channel 1		2		3		4		5	
Scheme	NLR	R	NLR	R	NLR	R	NLR	R	NLR	R
II	4×10^{-35}	11	1×10^{-36}	11	7×10^{-40}	11	1×10^{-52}	11	1×10^{-60}	11
III	1×10^{-13}	10	1×10^{-6}	9	1×10^{-27}	10	5×10^{-16}	10	3×10^{-15}	10
IV	3×10^{-9}	9	9×10^{-5}	8	1×10^{-20}	9	8×10^{-13}	9	7×10^{-13}	9
V	5×10^{-5}	7	1×10^{-3}	6	7×10^{-16}	7	1×10^{-7}	6	4×10^{-5}	7
VI	1×10^{-3}	5	6×10^{-3}	4	7×10^{-16}	8	1×10^{-7}	7	4×10^{-5}	8
VII	0·017	4	2×10^{-3}	5	1×10^{-8}	3	2×10^{-3}	4	0·013	4
VIII	2×10^{-7}	8	5×10^{-7}	10	7×10^{-13}	6	5×10^{-8}	8	1×10^{-3}	6
IX	5×10^{-4}	6	1×10^{-3}	7	6×10^{-10}	5	8×10^{-5}	5	3×10^{-3}	5
X	0·024	3	0·016	3	1×10^{-8}	4	4×10^{-3}	3	0·02	3
XI	0·26	2	0·026	1	8×10^{-5}	1	0·081	2	0·17	2
XII	0·34	1	0·028	1	8×10^{-5}	2	0·090	1	0·20	1

NLR is the ratio of the likelihood of the indicated scheme to the likelihood of the theoretical best fit to the distributions determined with sums of exponentials using all free parameters. The NLR is normalized to what would be observed for 1000 intervals. The rankings are based on the Schwarz criterion which applies a penalty for additional free parameters (eqn (3) in Methods). For channel 2, the Schwarz criterion for schemes XI and XII were the same.

scheme is only 1% of the probability (density) that the experimental data were drawn from the distributions predicted by the theoretical best description of the experimental data per 1000 events. Kinetic schemes with normalized likelihood ratios as small as 0·01 or even 0·0001 per thousand events could give what would be considered by visual evaluation to be reasonable descriptions of the distributions. The reason for this is that a NLR of 0·0001 per 1000 events becomes 0·99 for a single event ($0{\cdot}0001^{0{\cdot}001}$), suggesting an average likelihood difference per event of only 1% between the fit by the kinetic scheme and the theoretical best fit. However, even with a 1% likelihood difference per event, some visual differences between the predicted and experimental distributions were usually apparent, even on log–log plots, because the error for some parts of the distributions could be many times greater than the average error, and because the likelihood differences per event typically translate into plotted differences of greater magnitude than the likelihood differences per event.

Table 2 presents the normalized likelihood ratios for schemes II–XII for channels 1–5. Table 2 also presents the rankings of the various schemes based on the Schwarz criterion (Schwarz, 1987; Ball & Sansom, 1989), which applies a penalty for increased numbers of free parameters (eqn (3) in Methods).

The normalized likelihood ratios indicated that scheme XII with ten states typically gave the best description of the experimental data, followed by scheme XI with nine states and then scheme X with eight states. In contrast, the normalized likelihood ratios for scheme II with only four states were typically thirty to sixty

orders of magnitude smaller than the normalized likelihood ratios for schemes X–XII.

The rankings of the schemes in Table 2 by the Schwarz criterion were generally consistent with the normalized likelihood ratios. Schemes X, XI, and XII still typically ranked the highest, but the average rankings for schemes XI and XII were more similar because of the penalty for the additional state and transition pathways in scheme XII; scheme X still typically ranked third. The added penalty in the Schwarz criterion for additional states and pathways also had little effect on the rankings of the schemes with limited numbers of states, as schemes II and III with only four and five states, respectively, still typically ranked the lowest.

Some general observations can be drawn about gating mechanism from the results in Table 2 and the analysis of some other models not included in Table 2. Models which allowed direct transitions between open states, such as scheme X, were more likely than models which did not, such as scheme IX. A similar observation has been made for schemes XI and XII by modifying these schemes so that transitions cannot occur directly between open states. Models with one transition pathway between open and shut states, such as scheme VIII, give poorer descriptions of the data than models with the same number of states but with multiple transition pathways between open and shut states. Starting with a model with three shut and two open states, adding one or two additional shut states increased the likelihood more than adding one or two additional open states.

Schemes X–XII describe the Ca^{2+}-dependent shift in kinetics

Since even the top ranked schemes in Table 2 gave less than the theoretical best description of the data, it is necessary to determine whether these schemes can account for the major features of the Ca^{2+}-dependent kinetics before they might be considered as working hypotheses for channel gating.

The dashed line in Fig. 3*A* shows that scheme X correctly predicted the almost 400-fold change in P_{open} for channel 1 as a function of $[Ca^{2+}]_i$. The dashed lines in Figs 5 and 6 show that scheme X also accounts for most of the major features of the Ca^{2+}-dependent shifts in the dwell-time distributions for the same channel over the same 400-fold range in P_{open}. Note that the ability to predict the Ca^{2+}-dependent shifts in both P_{open} and the distributions arises solely as a consequence of the changes in $[Ca^{2+}]_i$ used to multiply the indicated forward rate constants in scheme X. The Ca^{2+}-dependent rate constants before multiplication and all of the other rate constants were the same for each of the different $[Ca^{2+}]_i$, and are listed in Table 1 under channel 1. It was also found for channel 1 that rate constants obtained by fitting the distributions obtained at only the highest and lowest $[Ca^{2+}]_i$ could then describe the distributions obtained at the two intermediate $[Ca^{2+}]_i$ for this channel. The distributions at the intermediate $[Ca^{2+}]_i$ were thus described without any free parameters.

Scheme X also described the major features of the Ca^{2+}-dependent shifts in kinetics for the other four channels with errors that could be somewhat more or less than those for channel 1, depending on the channel and the feature being examined. Examples of the ability of scheme X to predict the Ca^{2+}-dependence of P_{open} for channels 2 and 3 are shown by the dashed lines in Fig. 3*B* and *C*.

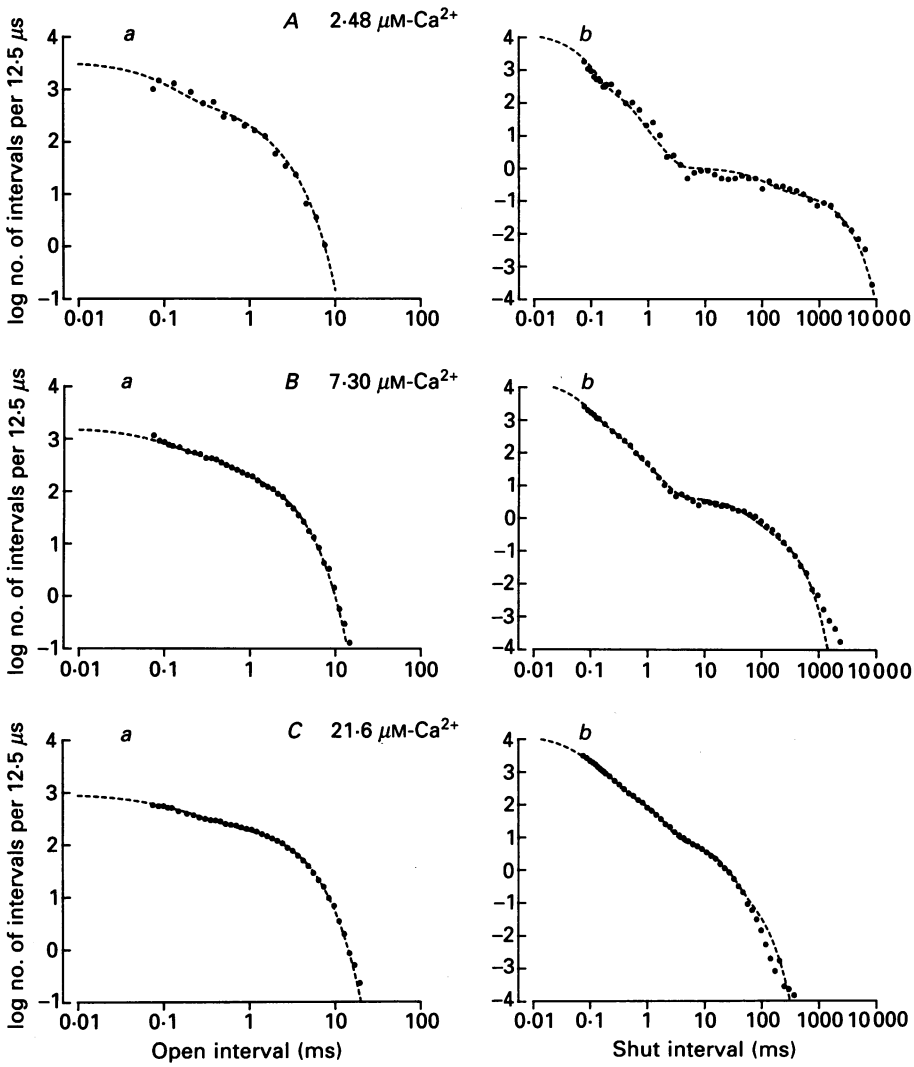

Fig. 6. Predicting the Ca^{2+} dependence of the dwell-time distributions. ●, experimentally observed dwell-time distributions. The dashed lines plot the distributions predicted by scheme X with the rate constants in Table 1. The experimental details are the same as for Fig. 4. Channel 1.

Schemes XI and XII have one and two more states, respectively, than scheme X, and gave slightly better descriptions (not shown) of the Ca^{2+}-dependent kinetics than those presented for scheme X in Fig. 6. A slightly better description is consistent with the higher normalized likelihood ratio for these schemes in Table 2. The improved description with schemes XI and XII was mainly with the intermediate to long shut intervals. However, none of the schemes adequately described the very longest (inactive) shut intervals when they were present in a distribution. Such inactive shut intervals typically occurred at a rate of about 0–2 per 100000 intervals, and were not present in about half of the shut distributions.

Apparent co-operative Ca^{2+} binding for schemes X–XII

For scheme X with four Ca^{2+} bindings, the average binding rates for the five channels for the first to fourth Ca^{2+} bindings to open and closed states were about 1·6, 10, 600 and 130 μM^{-1} s^{-1} (calculated from Table 1), suggesting that the effective binding of the second and third Ca^{2+} becomes increasingly faster, with the fourth binding still being many times faster than the first two. A similar type of accelerated (apparent co-operative) binding was observed for schemes XI and XII with five Ca^{2+} bindings. For these schemes the binding rates increased progressively for the second and third Ca^{2+}, with the binding rates for the fourth and fifth Ca^{2+} still many times faster than the first.

An assumption of identical and non-co-operative Ca^{2+} binding sites is inconsistent with the data

The observation that the estimated binding rates increased with the number of bound Ca^{2+} suggests some form of co-operative interaction among binding sites. Such an observation does not, however, exclude the possibility that the data might be equally well described by a simpler model of non-co-operative (independent) and identical Ca^{2+} binding sites. To examine this possibility the rate constants for Ca^{2+} binding and unbinding were constrained in various ways during the simultaneous fitting of distributions obtained at three to four different $[Ca^{2+}]_i$, and the best descriptions of the distributions were then compared to those obtained when fitting with unconstrained rate constants. Unconstrained rate constants allow co-operative binding.

In order to constrain scheme X for independent and identical Ca^{2+} binding sites, the rate constants for the first to fourth Ca^{2+} bindings were set to 4α, 3α, 2α and α, respectively, and the rate constants for the first to fourth Ca^{2+} unbindings were set to 4β, 3β, 2β and β, respectively. These constraints applied to Ca^{2+} bindings to both closed and open states, and α and β were free parameters. The normalized likelihood ratios per 1000 events (eqns (1) and (2) in Methods) for scheme X with the constraint of identical and independent Ca^{2+} binding sites were 5×10^{-22} for channel 1 and 2×10^{-12} for channel 2. The values may be compared to the much more favourable values of 0·023 and 0·016 when co-operative binding was allowed (Table 2, scheme X). These values for the normalized likelihood ratios indicate that the probability (density) that the experimental data were generated by scheme X was ten to twenty orders of magnitude less when the Ca^{2+} binding sites were constrained to be identical and independent than when co-operative Ca^{2+} binding was allowed. With identical and independent Ca^{2+} binding sites, scheme X ranked next to the worst scheme in Table 2 and gave very poor descriptions of the distributions (not shown). Thus, the possibility of identical and independent Ca^{2+} binding sites for scheme X can be rejected.

Predicting the durations of adjacent intervals with schemes X–XII

Schemes X–XII make predictions about gating that can be tested by examining the relationships between the durations of adjacent open and shut intervals. Some insight into the predicted relationships can be obtained from the lifetimes of the

states and the connections among the states. Schemes X(1) and X(15) present the predicted mean lifetimes (in ms) for the open and shut states for scheme X with 1 and 15 μM $[Ca^{2+}]_i$. The value listed by each state is the average of the predicted mean lifetimes of that state for all five channels. The values were calculated from the rates in Table 1 together with the indicated $[Ca^{2+}]_i$. (The mean lifetime of a state is given by the inverse of the sum of the rate constants leading away from the state.)

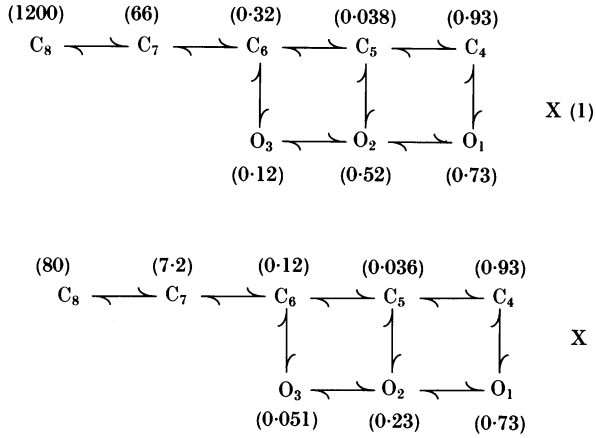

The predicted mean lifetimes of the closed states for scheme X(1) with 1 μM $[Ca^{2+}]_i$ decreased from 1200 to 0·038 ms as the states progressed from C_8 to C_5, and then increased to 0·93 ms for C_4. The mean lifetimes of the open states increased from 0·12 to 0·73 ms as the states progressed from O_3 to O_1. The same general relationship among the predicted mean lifetimes of the states was obtained with 15 μM $[Ca^{2+}]_i$, except that the mean lifetimes of C_8–C_6 and O_3 and O_2 were briefer.

The same general trend in lifetimes was also found for schemes XI and XII. The mean lifetimes of the shut states typically decreased from left to right, with the rightmost shut state increased in duration. The mean lifetimes of the open states typically increased from left to right.

McManus *et al.* (1985) observed an inverse relationship between the durations of adjacent open and shut intervals, and suggested that such a relationship would be consistent with scheme I if the mean lifetimes of the shut states decreased from left to right and the mean lifetimes of the open states increased from left to right. The lifetimes of the states for schemes X–XII are generally consistent with this suggestion, with the exception of the increased lifetime of the rightmost shut state (C_4). Thus, whereas schemes X–XII might predict a general inverse relationship between the durations of adjacent open and shut intervals because the longer lifetime shut states (or compound shut states) tend to be adjacent to the briefer lifetime open states, these schemes also predict that there may be an excess of longer open intervals (arising from O_1 and the compound open state O_2–O_1) adjacent to shut intervals of intermediate duration (arising from the rightmost shut state C_4).

Thus, if schemes X–XII capture the essential features of the gating, then the experimental data should also show, in addition to the general inverse relationship,

an excess of longer duration open intervals adjacent to shut intervals of intermediate duration.

To examine this possibility, plots of experimentally observed adjacent interval durations are presented in Fig. 7*A* and *B* as filled circles for channels 1 and 2. The

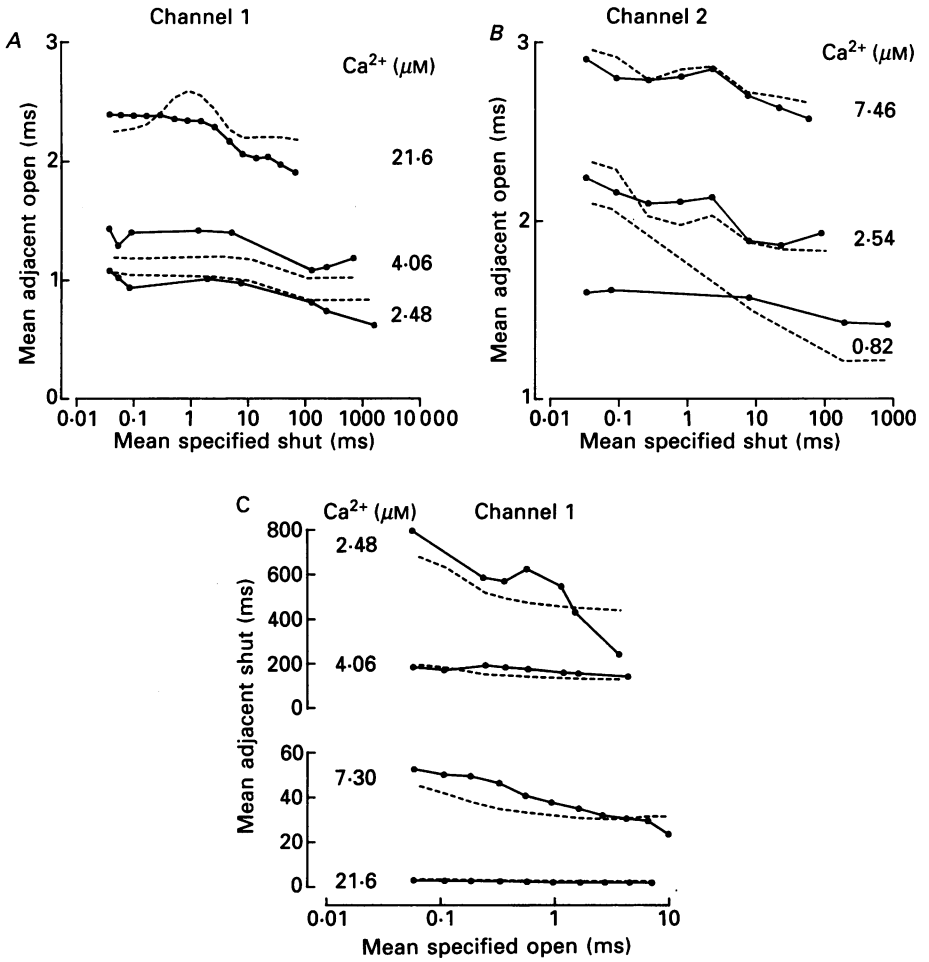

Fig. 7. Predicting the Ca^{2+} dependence of the adjacent interval durations. *A* and *B*, adjacent intervals plots of the mean durations of open intervals immediately preceding and following shut intervals of the specified durations (see Methods). Plots are presented at three different $[Ca^{2+}]_i$ for channels 1 and 2. ●——●, experimental observations. The predicted adjacent interval plots for scheme X with the rate constants in Table 1 are indicated by the dashed lines. *C*, experimental (●) and predicted (dashed lines) adjacent interval plots of the mean durations of shut intervals adjacent to open intervals of the specified durations for channel 1 for four different $[Ca^{2+}]_i$.

abscissa plots the mean durations of shut intervals of various specified durations, and the ordinate plots the mean durations of those open intervals that are adjacent to (immediately precede and follow) the shut intervals of specified durations (see Methods). Such adjacent interval plots are presented for data obtained at three

different $[Ca^{2+}]_i$ for each channel. Increasing $[Ca^{2+}]_i$ increased the mean lifetimes of the open intervals, as indicated by the upward shifts of the separate adjacent interval plots obtained at increasing $[Ca^{2+}]_i$. For example, for channel 1 the mean open intervals increased from about 0·6–1·0 ms at 2·48 μM $[Ca^{2+}]_i$ to about 1·9–2·4 ms at 21·6 μM $[Ca^{2+}]_i$. Increasing mean open times with increasing $[Ca^{2+}]_i$ is a common feature of maxi K^+ channels (Magleby & Pallotta, 1983*a*; Moczydlowski & Latorre, 1983).

A general inverse relationship between the durations of adjacent open and shut intervals is also apparent in Fig. 7*A* and *B*; at a given $[Ca^{2+}]_i$, open intervals adjacent to briefer shut intervals are generally longer than open intervals adjacent to longer shut intervals. The plots also show an excess of longer open intervals adjacent to shut intervals of intermediate duration, as indicated by the bump or plateau in the mean adjacent open intervals for specified shut intervals 1–5 ms in duration.

The predicted adjacent interval plots (dashed lines) were calculated by simulation with scheme X using the most likely rate constants in Table 1 for each channel (see Methods). In general, scheme X predicted the major features of the plots, including the large shifts in the mean open interval duration with $[Ca^{2+}]_i$, the general inverse relationship between the durations of adjacent open and shut intervals, and the excess of longer open intervals adjacent to shut intervals of intermediate duration. In some cases scheme X predicted too much excess; in others it accurately predicted the excess. A similar ability of scheme X to describe such adjacent interval plots was observed for the other three channels. As was the case in Fig. 7*A* and *B*, in some cases the predicted plots gave reasonable descriptions of the experimental data and in others there could be appreciable differences, but the differences were not consistent among the different channels.

Figure 7*C* presents adjacent interval plots of mean shut intervals adjacent to open intervals of specified duration (rather than of open intervals adjacent to specified shut intervals, as was the case in Fig. 7*A* and *B*). Plots are presented for channel 1 for data obtained at each of four different $[Ca^{2+}]_i$ (●). The decrease in mean shut interval with increasing $[Ca^{2+}]_i$ is clearly evident from the pronounced downward shift in the plots as the $[Ca^{2+}]_i$ is increased. The inverse relationship between adjacent open and shut intervals is apparent at the lower $[Ca^{2+}]_i$ and is masked at the highest $[Ca^{2+}]_i$ by the compressed ordinate. Scheme X approximated the Ca^{2+}-dependent shifts in mean shut intervals as well as the inverse relationship between adjacent interval durations (dashed lines in Fig. 7*C*). Similar results were found for the other four channels and for schemes XI and XII.

This section shows that schemes X–XII can predict the major features of the experimentally observed relationships between the durations of adjacent open and shut intervals, as expressed in adjacent interval plots. Since the rate constants used in the predictions were obtained by fitting dwell-time distributions (where open and shut intervals are separate) and not adjacent interval plots, the predictions were made without free parameters.

Uncertainty in estimates of rates constants

Inspection of the rate constants in Table 1 indicates variation among the rate constants obtained from the different channels. Such variation could arise from a

number of factors such as: (1) inability of the fitting process to find the most likely solution for each channel; (2) stochastic variation in dwell-time distributions due to limited sample sizes; (3) insufficient information in the fitted data to define some of the rate constants; (4) errors associated with the assumption of idealized filtering used to correct for missed events (see Methods); (5) noise in the single-channel current record; (6) experimental errors, such as those associated with estimating free $[Ca^{2+}]$; and (7) differences among the different channels or in the channel environments in the different excised patches of membrane.

The variation in rate constants among channels for scheme X is unlikely to arise from factor (1) above, since repeated simultaneous fitting of the same data sets, but with different initial parameters gave most likely rate constants which typically varied less than 1%. Thus, the fitting process appears to find the peak of the likelihood surface.

Estimates of the uncertainty in rate constants which could arise from the combined factors (1)–(3) above were made using resampling (see Methods). The uncertainty for channels 1 and 2 is indicated by the standard deviations in Table 1. The standard deviation with resampling was typically about 1–15% of the mean, depending on the rate, although some rates, such as k_{2-3} and k_{3-2} for channel 1 and k_{1-4} and k_{4-1} for channel 2 were less well defined.

An estimate of the uncertainty in rate constants which could arise for scheme X from the combined factors (1)–(5) above was made for channel 1 using single-channel data simulated with scheme X using the rates in Table 1. The simulated single-channel currents included the true effects of filtering and noise (McManus *et al.* 1987; Magleby & Weiss, 1990*a*) in order to take into account errors that might arise from factors (4) and (5) above. The numbers of simulated events for the four different $[Ca^{2+}]_i$ were the same as in the experimental data. The simulated single-channel currents were threshold sampled and binned into dwell-time histograms as was done for the experimental data. The simulated dwell-time distributions were then simultaneously fitted assuming idealized filtering and no noise, as was done for the experimental data, and the maximum likelihood estimates of the rate constants compared to the rate constants used to simulate the current records. If there were no errors in the analysis from any source and if the data were sufficient to define all the rate constants, then the rate constants recovered by measuring and fitting the simulated current records should be the same as those used to simulate the current records.

The average error from the combined factors (1)–(5) for thirteen of the eighteen rate constants for scheme X was 5·5% (range 1–12%). Rate k_{3-6}, which would be especially sensitive to filtering and noise because of the brief lifetime of state O_3 and the infrequent entries to this state, had an error of about 25%. Rates k_{2-3} and k_{3-2} had values of 3·79 and 52·3 s^{-1}, and rates k_{4-5} and k_{5-4} had values of 71·8 and 10·9 s^{-1}. Further simulations indicated that rates k_{2-3}, k_{3-2}, k_{4-5}, and k_{5-4}, all of which are in loops, were poorly defined; they could vary within the range of about 0–80 s^{-1} with minimal effects on the distributions, provided that minor compensating changes occurred in some of the other rates.

Examination of the rates in Table 1 for all five channels suggests that only a small fraction of the total transitions among states would occur between O_2 and O_3 or

between C_4 and C_5. The limited number of transitions on these pathways would contribute to the poor definition of these rates. Consistent with limited transitions, the rate constants between O_2 and O_3 for all channels and between C_4 and C_5 for all channels except channel 2 could be set to zero during the fitting with insignificant or just significant ($P < 0.05$) effects on the likelihoods, depending on the channel (likelihood ratio test, which applies a penalty for additional free parameters; Rao, 1973).

Interestingly, resampling was insufficient to indicate that some of the rate constants in the loops were poorly defined. Instead, the perturbation of the estimation process by measuring and fitting simulated current records with noise and filtering suggested the poor definition, which was then verified, as indicated above, by fixing the rates to various values during the fitting.

It is necessary to correct for missed events

All of the kinetic analysis presented in this paper was carried out with (approximate) corrections for missed events (see Methods). Nevertheless, it was of interest to determine what additional errors in estimates of rate constants might occur if no corrections for missed events were applied, since much of the published kinetic analysis is without correction. Fitting scheme X to experimental and simulated data for channel 1 without corrections for missed events indicated that failure to apply a correction would have increased the average error in estimating the fourteen well-defined rate constants 3-fold (from 5·5 to 16%), with some large absolute errors (70–85%) in some of the well-defined rate constants, such as $k_{2\text{-}5}$.

Schemes X–XII do not give the theoretical best fit to the data

Scheme X has been presented in detail since it is the simplest gating mechanism that can account for the major features of the Ca^{2+}-dependent kinetics for all five channels. Schemes XI and XII then gave somewhat better descriptions of the dwell-time distributions. However, the normalized likelihood ratios in Table 2 and the plots in Figs 3–7 indicate that none of these schemes described the data as well as is theoretically possible (see Methods). Comparison of likelihood estimates from the simultaneous fitting of data obtained from simulated current records to the likelihood estimates obtained from the theoretical best description of the same simulated data, indicated that errors arising mainly from stochastic variation, imperfect corrections for missed events, and noise would be expected to reduce estimates of the normalized likelihood ratio from 1·0 to about 0·8–0·9, even if the schemes were correct. This reduction would be insufficient to account for the less than theoretical best fits for schemes X–XII (Table 2). Less than theoretical best fits could arise from experimental errors such as minor drift in the channel properties or small errors in estimating the free $[Ca^{2+}]_i$. Alternatively, less than theoretical best fits could arise because the actual gating mechanism may be more complex than the examined schemes, as considered below.

More complex schemes

Estimates of the number of kinetic states for the maxi K^+ channel, obtained by fitting dwell-time distributions with sums of exponentials, indicate at least three to

four open states and states and five to eight shut states (McManus & Magleby, 1988), suggesting that there may be more kinetic states than contained in schemes X–XII. Consequently, schemes with increased numbers of states were examined. Increasing the number of open and/or shut states could improve the description of the dwell-time distributions over that obtained with schemes X–XII. For example, an extension of scheme XII to seven shut states and four open states gave a normalized likelihood ratio of 0·45 for channel 2 and an excellent description of the dwell-time distributions. However, for the more complex models, the gating mechanisms associated with the best likelihoods could be different for the different channels. For example, the optimal number of Ca^{2+} binding steps and the location of these steps for more complex models could be different for the different channels. Thus, while more complicated models can give better fits than schemes X–XII, it is difficult to present a definitive model. Nevertheless, two common features of the more complex models are worth noting

In general, the more likely complex models were extensions of schemes X–XII. Thus, the mean lifetimes of the open states typically increased from left to right and the mean lifetimes of the shut states typically decreased from left to right, except that the rightmost state usually had a longer lifetime of about 1 ms. For all channels except channel 3, which had a Hill slope greater than four, models with six or more shut states, but only four Ca^{2+} binding sites, typically gave better likelihoods than models with five Ca^{2+} binding sites. Further examination of more complex models seems best delayed until more powerful fitting techniques (Magleby & Weiss, 1990*a*, *b*), which directly take into account the correlation information as well as the true effects of filtering and noise, can be used.

DISCUSSION

This study develops kinetic gating mechanisms that can account for the major features of the Ca^{2+}-dependent kinetics of large-conductance Ca^{2+}-activated K^+ channels from rat skeletal muscle. Kinetic schemes are presented that can account for the Ca^{2+}-dependent shifts in both P_{open} and the dwell-time distributions for changes in $[Ca^{2+}]_i$ which change P_{open} up to 400-fold (Figs 3 and 6). In addition, the gating mechanisms can predict (approximately) the relationships between the durations of adjacent open and shut intervals as well as the Ca^{2+}-dependent shifts in these relationships (Fig. 7).

Simple models can describe the major features of Ca^{2+}-dependent gating

The simplest gating mechanism that could account for the major kinetic features of Ca^{2+}-activation was a model with three open and five shut states and four Ca^{2+} binding sites (scheme X). Increasing the number of shut states to six and increasing the number of open states to four could give even better descriptions of the experimental data (schemes XI and XII; Table 2).

Although models with eight to ten states may not appear simple, the possibility existed that much more complicated models might have been needed. The reason for this is that gating mechanisms that allow the binding of four Ca^{2+} ions can have many more kinetic states than the eight states in scheme X, provided that the

different binding sites, or combinations of sites, have different binding properties and/or convey different kinetic properties on the channel. Figure 8 shows why this is the case by presenting the kinetic scheme for a model which has four different Ca^{2+} binding sites (labelled 1–4), with any unbound site capable of binding Ca^{2+}. For this

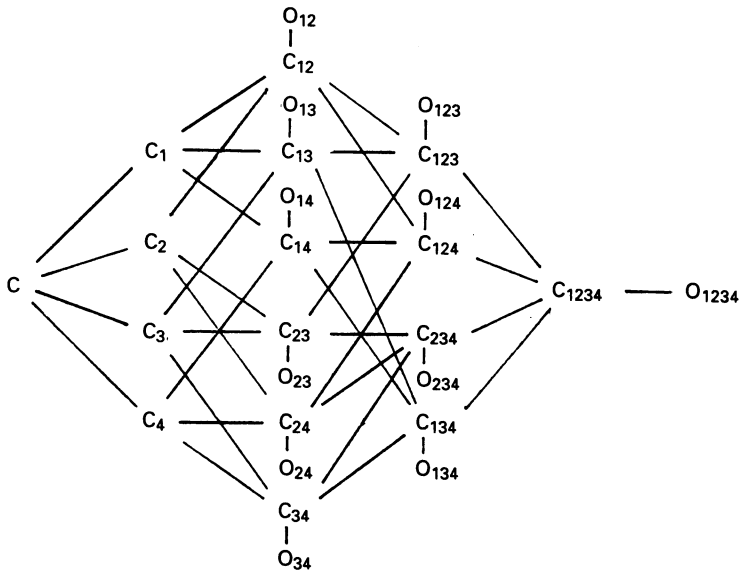

Fig. 8. Hypothetical kinetic scheme for a channel with four independent Ca^{2+} binding sites, each of which impart different kinetic properties on the channel. The sites are numbered 1–4 and listed when a Ca^{2+} is bound to that site for closed (C) and open (O) states. Opening can occur with two, three or four bound Ca^{2+}. For simplicity, transitions between the open states have not been included.

model, in which openings can occur with two to four bound Ca^{2+}, there would be sixteen shut states and eleven open states. (For simplicity, possible transitions between open states have not been indicated.) If Ca^{2+} bindings to the different sites or combinations of sites imparts sufficiently different lifetimes to the states with different sites bound, then the different states in Fig. 8 could be detected as different kinetic states.

Our observations of typically three to four detected open states and five to eight detected shut states (McManus & Magleby, 1988), and that schemes X–XII with three to four open and five to six shut states can describe the major kinetic features of the Ca^{2+} activation of the channel, contrast with the large numbers of states predicted by the gating mechanism in Fig. 8. Thus, either there are fewer states than in Fig. 8, or many of the states have similar kinetic properties and are not detected. On this basis, the complex scheme in Fig. 8 would reduce to the simpler scheme X if the kinetic properties of the states were determined solely by the number of bound Ca^{2+}, as would be the case for equivalent sites. The complex scheme in Fig. 8 could also reduce to scheme X for non-equivalent sites if the binding of Ca^{2+} to the non-equivalent sites were strictly sequential (1–4), so that there would be only one configuration of the channel for each of the different numbers of bound Ca^{2+}.

Although schemes X–XII would be preferred over more complex schemes like the

one in Fig. 8, it is possible that the inability of the simpler schemes to give theoretically perfect descriptions of the data arises because the gating has some of the features of the more complex schemes. The scheme in Fig. 8 also has some features in common with the lattice type gating mechanisms considered by Lauger (1988). The possible relationship between discrete state models, such as schemes II–XII, and diffusion type models (Millhauser, Salpeter & Oswald, 1988) has been considered previously (McManus & Magleby, 1989).

Apparent co-operative Ca^{2+} binding for schemes X–XII

If the unbound sites in schemes X–XII are equivalent, then the progressively increasing rates for binding of the first, second and third Ca^{2+} of 1·6, 10, and 600 μM^{-1} s^{-1} for scheme X (average of channels 1–5 for both open and shut states, Table 1) would require that the binding of a Ca^{2+} to any one of the unbound sites changes the binding properties of all the remaining sites in a co-operative manner. Such co-operative interaction between equivalent sites would be difficult to distinguish from strictly sequential binding to sites with different properties. Sequential binding could occur if the binding at a site induced a conformational change which either exposed the next site or increased the binding constant of the next site from a negligible value. Thus, sequential binding could also have co-operative interactions, but the order of binding would always be the same.

If the Ca^{2+} binding sites are equivalent with co-operative interaction, than the actual rate constant for each binding site would depend on the number of bound Ca^{2+} and would be given by the values in Table 1 divided by the number of unbound sites. If Ca^{2+} binding occurs in strict sequence, then the rate constants in Table 1 indicate the rate constant for each step in the sequence. Knowledge of the subunit and binding site structure of K^+ channels could help resolve the question of equivalent sites with co-operative interaction or sequential binding.

Some limitations of the considered gating mechanisms

The considered kinetic schemes have a number of limitations. They do not take into account the possibility that the concentration of Ca^{2+} at the binding sites may not be the same as in the bulk solution (Moczydlowski & Latorre, 1983). If the different Ca^{2+} binding sites are at different depths in the electric field of the membrane, or if there are differences in charge density near the binding sites, then the Ca^{2+} concentration will be different at the different sites (e.g. Dani, 1986). The considered schemes do not account for the voltage sensitivity of the gating of the channel, which has been considered in models by Moczydlowski & Latorre (1983) and Methfessel & Boheim (1982). The considered schemes do not account for infrequent entries into the long-lasting inactive shut state, as studied by Pallotta (1985). The considered schemes also do not account for the infrequent shifts into kinetic modes other than normal, which include about 4% of the intervals (McManus & Magleby, 1988). Some possible mechanisms for moding were considered by McManus & Magleby (1988), and the scheme in Fig. 8 suggests additional possibilities for other kinetic modes; an infrequently occurring combination of bound sites might give rather different kinetic properties to the channel, producing an apparent shift to a different kinetic mode.

Working hypothesis for Ca^{2+}-dependent gating

Schemes X–XII provide simplified working hypotheses for the Ca^{2+}-dependent kinetics during normal activity. The basic gating mechanism of these schemes is the same. Increasing Ca^{2+} drives the channel away from the longer shut states towards

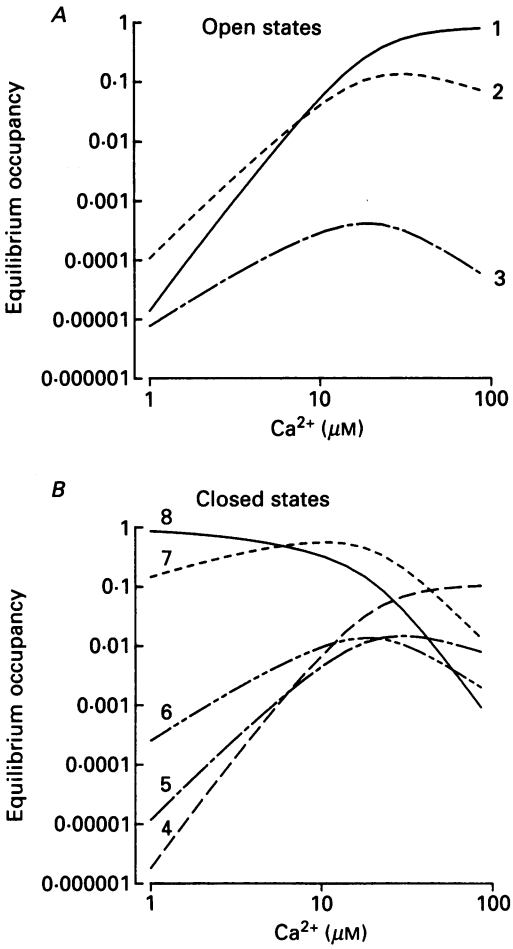

Fig. 9. Equilibrium occupancy of the open (*A*) and closed (*B*) states for channel 1, as predicted by scheme X. The numbering of the states and the rate constants used in the prediction are given in Table 1.

the briefer shut states and the open states. This is detailed in Fig. 9 for scheme X, where the predicted equilibrium occupancy of the three open (*A*) and five shut (*B*) states is presented as a function of $[Ca^{2+}]_i$. The rate constants used in the calculations are from channel 1 in Table 1 and the method of numbering the different states is also defined in Table 1.

At the low Ca^{2+} of 1 μM, which gives a predicted P_{open} of only 0·00013, all three open states are still entered, but the percentage of time spent in the open states is minimal. Most (88%) of the time is spent in the longest shut state C_8. As $[Ca^{2+}]_i$ is increased,

occupancy is shifted towards the longest lifetime open state O_1 and away from the longest lifetime shut state C_8. At 86 μM-Ca^{2+} (extreme right), the calculated P_{open} is 0·87, with 80% of the time spent in state O_1, and only 0·025% spent in C_8.

Notice in Fig. 9 that the Ca^{2+} dependence of the equilibrium occupancy for any given state depends on the number of Ca^{2+} bindings required to reach that state. For example, the open state O_3 requires the fewest (two) bound Ca^{2+} to be reached and has the lowest Ca^{2+} dependence, (the lowest slope). In contrast, the open state O_1 requires the most (four) bound Ca^{2+} to be reached and has the highest Ca^{2+} dependence. This prediction of scheme X is consistent with the experimental observations presented in Fig. 2 of Magleby & Pallotta (1983*a*). They found that the frequency of openings to the briefest lifetime open component increased approximately linearly with $[Ca^{2+}]_i$ and then decreased as $[Ca^{2+}]_i$ was further increased, similar to what is observed for states O_2 and O_3 in Fig. 9*A*. They also found that the frequency of openings to the longest open component was much more Ca^{2+} dependent and continued to increase as Ca^{2+} was increased, just as it observed for state O_1 in Fig. 9*A*.

From Fig. 9 it can also be seen that the predicted limit on P_{open} at high Ca^{2+} is determined mainly by entries into state C_4, which has a lifetime of about 1 ms, raising the possibility that C_4 might be a blocked state of the channel. Blocked states, although with longer lifetimes, have been observed at high $[Ca^{2+}]_i$ (Vergara & Latorre, 1983). Further tests of the schemes presented here would be to examine the detailed kinetics at high $[Ca^{2+}]_i$ to see if the predictions of Fig. 9 at high values of P_{open} are consistent with the experimental observations.

Scheme X allows many different sequences of transitions between the open and closed states. Examination of rates for scheme X in Table 1 suggests a main gating pathway among these many possibilities. Starting with no bound Ca^{2+}, the closed channel will typically bind three Ca^{2+}, open and then bind an additional Ca^{2+} (C_8–C_7–C_6–C_5–O_2–O_1). The channel would typically release bound Ca^{2+} in the reverse order. The steep relation between $[Ca^{2+}]_i$ and P_{open} (Hill slopes of $\sim$ 3–4) is explained by the observation that the channel typically binds three Ca^{2+} before opening and remains open longer if a fourth Ca^{2+} binds to the open state.

A simple physical interpretation consistent with many of these observations is that the binding of each additional Ca^{2+} to the closed conformation puts the channel under increasing strain, which favours both the binding of additional Ca^{2+} and the transition to the open conformation. Opening then relieves the strain. The unbinding of Ca^{2+} from the open conformation then reintroduces the strain, favouring the transition back to the closed conformation. Such a model is similar to the oxygen-induced conformation change in haemoglobin (Dickerson & Geis, 1983).

General similarity in gating mechanism for the five channels

The five single maxi K^+ channels studied in detail were similar, in that they all increased P_{open} with increasing $[Ca^{2+}]_i$ (Fig. 3), and the general form of the dwell-time distributions and the Ca^{2+}-dependent shifts in the distributions were also similar, suggesting a similar gating mechanism for all five channels. There were, however, some specific differences in the Hill plots (Fig. 3) and other Ca^{2+}-dependent kinetics for the channels (compare *A* and *B* of Fig. 7). The rate constants in Table 1 reflect both these similarities and differences among the channels.

Although there are some specific differences in the rate constants from channel to

channel, the general trends in relative magnitudes of the various rate constants are similar. Rate constants that are fast (or slow) for one channel are typically fast (or slow) for the other channels as well. For example, k_{5-2} is one of the fastest rate constants for all five channels and k_{8-7} is one of the slowest. As another example, the rate for channel closing for all five channels decreases as more Ca^{2+} ions are bound to the open state, with k_{3-6} being the fastest, k_{2-5} intermediate, and k_{1-4} the slowest.

Superimposed on the general similarity in rate constants among the channels are some specific differences. For example, k_{5-6} is fast for all five channels, but varies about twofold among the channels. Calculations were performed to determine if any of the specific differences in rate constants between channels 1 and 2 were significant (see Methods). Of the eighteen rate constants, all but four (k_{2-1}, k_{4-5}, k_{6-3}, and k_{6-5}) were significantly different $P < 0{\cdot}05$). Some significant differences might have been expected since the Hill plots for channels 1 and 2 differ in slope and the value of $K_{0{\cdot}5}$ (Fig. 3).

A possible specific difference in gating for channel 2

Although scheme X gave similar descriptions of the Ca^{2+}-dependent kinetics for channels 1 and 2 (normalized likelihood ratios of 0·041 and 0·037), channel 2 differed from channel 1 and the other channels in an interesting way. For channel 2 there were negligible transitions between O_1 and C_4 (k_{1-4} and k_{4-1} were small) and appreciable transitions between C_4 and C_5, just the opposite of what was observed for the other channels. Negligible transitions between O_1 and C_4 for channel 2 would suggest that openings might not occur from C_4. Negligible transitions between C_4 and C_5 for the other channels would be consistent with C_5 being a blocking (or closing) of the open state O_1.

These differences in rate constants could reflect an actual difference in channel 2, or they might arise from errors inherent in the collection and analysis of the single-channel data. The most obvious possibility for the difference is that the estimated rate constants may not be most likely. Repeated fitting with widely different starting parameters, including those found for other channels, did not reveal a more likely solution for scheme X for either channel 2 or the other channels. Interestingly, a significantly less likely solution ($P \ll 0{\cdot}001$, likelihood ratio test) associated with a local maximum was found for channel 2 which was similar to that obtained for the other channels, in that there were appreciable transitions between O_1 and C_4 and negligible transitions between C_4 and C_5. Thus, it is possible that undetected drift or some other factor distorted the data sufficiently for channel 2 so that the most likely solution did not give the best representation of the actual gating mechanism. It is also possible, that some of the favoured transition pathways for channel 2 are different from the other channels. In either case, the relative lifetimes of the various states and the major features of the gating mechanism for channel 2 are similar to those for the other channel.

Comparison to previous studies

The working hypotheses presented by schemes X–XII in this paper for the Ca^{2+}-dependent gating of the large-conductance Ca^{2+}-activated K^+ channel in skeletal muscle extends those presented in previous studies. Moczydlowski & Latorre (1983)

found that the gating of maxi K^+ channels inserted into lipid bilayers was consistent with scheme II. The limited number of states in their scheme (two open and two shut), when compared to the more complex schemes needed to describe the data in our study, may be a consequence of the 3 ms effective time resolution in their study, when compared to the typically 30 μs time resolution in our study. With their greatly decreased time resolution, the briefer duration open and shut components would not have been resolved, but would be combined with the longer duration components. The decreased time resolution could also mask the dependent relationship between the durations of adjacent intervals that is observed when data are collected at higher time resolution (Fig. 7). This dependent relationship requires that there be two or more transition pathways between open and shut states (Fredkin *et al.* 1985; McManus *et al.* 1985; McManus & Magleby, 1989), in contrast to scheme II which was a single transition pathway. Notice that scheme II is contained within the main gating pathway for scheme X if some of the states in scheme X are combined. However, the additional states and Ca^{2+} bindings in scheme X are essential to account for the observed Hill slopes, the additional components in the high resolution distributions, and the dependent relationship between adjacent open and shut states.

Magleby & Pallotta (1983*a*, *b*), working with higher time resolution (0·15 ms) than the 3 ms of Moczydlowski & Latorre (1983), but less than the 30 μs in this study, found that the kinetics of maxi K^+ channels at a single Ca^{2+} could be approximated by scheme III. They also hypothesized from the Ca^{2+} dependence of the open distributions that there must be an additional open state, as indicated in scheme IV. Although Magleby & Pallotta found that scheme IV could describe many of the features of channel gating, including the Ca^{2+} dependence of the open distributions, they suggested that it was still too simple because some of the estimated rate constants for this scheme were found to change with $[Ca^{2+}]_i$.

Just as the four-state model of Moczydlowski & Latorre (1983) described by scheme II is contained within the more complex schemes X–XII, the five- and six-state models of Magleby & Pallotta (1983*a*) described by schemes III and IV are also contained within the more complex schemes developed in this study. Hence, the results of the present study are consistent with and extend the findings of these earlier studies. The improvement in the description of the data by the more complex schemes X–XII depends on how many events are used to compare the schemes. The normalized likelihood ratios in Table 2 give the ratios of the likelihood that the data were drawn from distributions generated by the indicated schemes to the likelihood that the data were drawn from distributions describing the theoretical best fit of the data. The normalized likelihood ratio values in Table 2 are normalized to 1000 events (eqns (1) and (2) in Methods). The values of the normalized likelihood ratios in Table 2 for schemes X–XII are about thirty to sixty orders of magnitude greater than the values for scheme II and about three to twenty-five orders of magnitude greater than the values for schemes III and IV. If the comparison were based on the typically 2×10^5 fitted events rather than the normalized value of 1000 events, then the improvement in likelihood values with schemes X–XII when compared to schemes II–IV would be thousands of orders of magnitude.

Alternatively, if the comparison among the schemes were based on the average

improvement in the likelihood of the fit for a single event, then the average likelihood ratio per event for the five channels for schemes II, III, IV, X, XI and XII would be: 0·9115, 0·9658, 0·97433, 0·9929, 0·9963 and 0·9964, respectively. Thus, schemes III and IV are 6–7% more likely per event than scheme II, and schemes X–XII are about 2% more likely per event than scheme IV.

Methfessel & Boheim (1982) proposed a model for gating of maxi K^+ channels in which Ca^{2+} binds to two sites: an activation site where Ca^{2+} binding leads to channel opening, and a site on a blocking particle where Ca^{2+} binding prevents the particle from blocking the channel. Since the analysis of Methfessel & Boheim (1982) was restricted to activity within bursts, their model would be too simple to account for our observations, which include all intervals during normal activity. For example, if the activation and blocking processes in their model are strictly coupled with activation preceding block, then their model reduces to a scheme similar to scheme II.

Conclusion

It is the simultaneous fitting of data obtained at three to four different $[Ca^{2+}]_i$ together with the increased time resolution and analysis of large numbers of events in the present study that has allowed us to develop gating mechanisms (schemes X–XII) that are orders of magnitude more likely than previously considered models (Table 2). However, just as the working hypotheses from previous studies have served as building blocks in the present study, the working hypotheses developed in the present study will also require modification when further detailed studies on gating are carried out. Nevertheless, schemes X–XII can account for the major features of the Ca^{2+}-dependent kinetics of maxi K^+ channels over a wide range of P_{open}, and likelihoods for these models start to approach those expected for a theoretical best description of the data. Thus, these schemes should serve as working hypotheses to explore the mechanisms by which various factors, such as Mg^{2+} (Golowasch *et al.* 1986), alter the kinetics of the channel. These schemes should also provide starting points for studies relating structure to kinetic mechanism, when the maxi K^+ channel becomes available for genetic manipulation.

This work was supported by grants to K.L.M. from the National Institutes of Health (AR-32805) and the Muscular Dystrophy Association. O.B.M. has received fellowships from the National Institutes of Health (NS 07044) and the Muscular Dystrophy Association.

REFERENCES

BALL, F. G. & SANSOM, M. S. P. (1989). Ion-channel gating mechanisms: model identification and parameter estimation from single channel recordings. *Proceedings of the Royal Society* B **236**, 385–416.

BALSER, J. R., RODEN, D. M. & BENNETT, P. B. (1990). Global parameter optimization for cardiac potassium channel gating models. *Biophysical Journal* **57**, 433–444.

BARRETT, J. N., MAGLEBY, K. L. & PALLOTTA, B. S. (1982). Properties of single calcium-activated potassium channels in cultured rat muscle. *Journal of Physiology* **331**, 211–230.

BATES, S. E., SANSOM, M. S. P., BALL, F. G., RAMSEY, R. L. & USHERWOOD, P. N. R. (1990). Glutamate receptor-channel gating. *Biophysical Journal* **58**, 219–229.

BAUER, R. J., BOWMAN, B. F. & KENYON, J. L. (1987). Theory of the kinetic analysis of patch clamp data. *Biophysical Journal* **52**, 961–978.

BLATZ, A. L. (1989). Large conductance Ca-activated K channels in adult rat diaphragm: single channel properties and block by protons. *Biophysical Journal* **55**, 545a.

BLATZ, A. L. & MAGLEBY, K. L. (1984). Ion conductance and selectivity of single calcium-activated potassium channels in cultured rat muscle. *Journal of General Physiology* **84**, 1–23.

BLATZ, A. L. & MAGLEBY, K. L. (1986*a*). Correcting single channel data for missed events. *Biophysical Journal* **49**, 967–980.

BLATZ, A. L. & MAGLEBY, K. L. (1986*b*). Quantitative description of three modes of activity of fast chloride channels from rat skeletal muscle. *Journal of Physiology* **378**, 141–174.

BLATZ, A. L. & MAGLEBY, K. L. (1989). Adjacent interval analysis distinguishes among gating mechanisms for the fast chloride from rat skeletal muscle. *Journal of Physiology* **410**, 561–585.

CHRISTENSEN, O. & ZEUTHEN, T. (1987). Maxi K^+ channels in leaky epithelia are regulated by intracellular Ca^{2+}, pH and membrane potential. *Pflügers Archiv* **408**, 249–259.

COLQUHOUN, D. (1971). *Lectures on Biostatistics*. Oxford University Press, London.

COLQUHOUN, D. (1973). The relation between classical and cooperative models for drug action. In *Drug Receptors*, ed. RANG, H. P., pp. 149–182. University Park Press, London.

COLQUHOUN, D. (1988). Single channel analysis costs time. *Trends in Pharmacological Sciences* **9**, 157–158.

COLQUHOUN, D. & HAWKES, A. G. (1977). Relaxation and fluctuation of membrane currents that flow through drug operated channels. *Proceedings of the Royal Society* B **199**, 231–262.

COLQUHOUN, D. & HAWKES, A. G. (1981). On the stochastic properties of single ion channels. *Proceedings of the Royal Society* B **211**, 205–235.

COLQUHOUN, D. & HAWKES, A. G. (1982). On the stochastic properties of bursts of single ion channel openings and of clusters of bursts. *Philosophical Transactions of the Royal Society* B **300**, 1–59.

COLQUHOUN, D. & HAWKES, A. G. (1983). The principles of the stochastic interpretation of ion channel mechanisms. In *Single-Channel Recording*, ed. SAKMANN, B. & NEHER, E., pp. 135–175. Plenum Press, New York.

COLQUHOUN, D. & HAWKES, A. G. (1990). Stochastic properties of ion channel openings and bursts in a membrane patch that contains two channels: evidence concerning the number of channels present when a record containing only single openings is observed. *Proceedings of the Royal Society* B **240**, 453–477.

COLQUHOUN, D. & SAKMANN, B. (1985). Fast events in single-channel currents activated by acetylcholine and its analogues at the frog muscle end-plate. *Journal of Physiology* **369**, 501–557.

COLQUHOUN, D. & SIGWORTH, F. J. (1983). Fitting and statistical analysis of single-channel records. In *Single-Channel Recording*, ed. SAKMANN, B. & NEHER, E., pp. 191–263. Plenum Press, New York.

COOK, D. L., IKEUCHI, M. & FUJIMOTO, W. Y. (1984). Lowering of pH inhibits Ca^{2+}-activated K^+ channels in pancreatic b cells. *Pflügers Archiv* **391**, 85–100.

DANI, J. A. (1986). Ion-channel entrances influence permeation. Net charge, size, shape and binding considerations. *Biophysical Journal* **49**, 607–618.

DICKERSON, R. E. & GEIS, I. (1983). *Hemoglobin: Structure, Function, Evolution, and Pathology*. Benjamin/Cummings Publishing Company, Inc., London.

DIONNE, V. E., STEINBACH, J. H. & STEVENS, C. F. (1978). An analysis of the dose–response relationship at voltage-clamped frog neuromuscular junctions. *Journal of Physiology* **281**, 421–444.

EFRON, B. (1982). *The Jackknife, the Bootstrap, and other Resampling Plans*. Society for Industrial and Applied Mathematics, Philadelphia.

FREDKIN, D. R., MONTAL, M. & RICE, J. A. (1985). Identification of aggregated Markovian models: application to the nicotonic acetylcholine receptor. In *Proceedings of the Berkeley Conference in Honor of Jerzy Neyman and Jack Kiefer*, ed. LECAM, L. M. & OLSHEN, R. A., pp. 269–289. Wadsworth Press, Belmont, CA, USA.

GIBB, A. J., KOJIMA, H., CARR, J. A. & COLQUHOUN, D. (1990). Expression of cloned receptor subunits produces multiple receptors. *Proceedings of the Royal Society* B **242**, 108–112.

GOLDMAN, L. (1991). On the extraction of kinetic rate constants from experimental data. *Biophysical Journal* (in the Press).

GOLOWASCH, J., KIRKWOOD, A. & MILLER, C. (1986). Allosteric effects of Mg^{2+} on the gating of Ca^{2+}-

activated K^+ channels from mammalian skeletal muscle. *Journal of Experimental Biology* **124**, 5–13.

HAMILL, O. P., MARTY, A., NEHER, E., SAKMANN, B. & SIGWORTH, F. J. (1981). Improved patch-clamp techniques for high-resolution current recording from cells and cell-free membrane patches. *Pflügers Archiv* **391**, 85–100.

HORN, R. (1987). Statistical methods for model discrimination: application to gating kinetics and permeation of the acetylcholine receptor channel. *Biophysical Journal* **51**, 255–263.

JACKSON, M. B., WONG, B. S., MORRIS, C. E. & LECAR, H. (1983). Successive openings of the same acetylcholine receptor channel are correlated in open time. *Biophysical Journal* **42**, 109–114.

KERRY, C. J., RAMSEY, R. L., SANSOM, M. S. P. & USHERWOOD, P. N. R. (1988). Glutamate receptor channel kinetics. The effect of glutamate concentration. *Biophysical Journal* **53**, 39–52.

KIENKER, P. (1989). Equivalence of aggregated Markov models of ion-channel gating. *Proceedings of the Royal Society* B **236**, 269–309.

KORN, S. J. & HORN, R. (1988). Statistical discrimination of fractal and Markov models of single channel gating. *Biophysical Journal* **54**, 871–877.

KUME, H., TAKAGI, K., SATAKE, T., TOKUNO, H. & TOMITA, T. (1990). Effects of intracellular pH on calcium-activated potassium channels in rabbit tracheal smooth muscle. *Journal of Physiology* **424**, 445–457.

LATORRE, R. & MILLER, C. (1983). Conduction and selectivity in potassium channels. *Journal of Membrane Biology* **71**, 11–30.

LATORRE, R., OBERHAUSER, A., LABARCA, P. & ALVAREZ, O. (1989). Varieties of calcium-activated potassium channels. *Annual Reviews of Physiology* **51**, 385–399.

LATORRE, R., VERGARA, C. & HIDALGO, C. (1982). Reconstitution in planar lipid bilayers of a Ca^{2+}-dependent K^+ channel from transverse tubule membranes isolated from rabbit skeletal muscle. *Proceedings of the National Academy of Sciences of the USA* **79**, 805–809.

LAUGER, P. (1988). Internal motions in proteins and gating kinetics of ionic channels. *Biophysical Journal* **53**, 877–884.

LAURIDO, C., WOLFF, D. & LATORRE, R. (1990). Effect of pH in a Ca^{2+}-activated K^+ channel [K(Ca)] from rat skeletal muscle. *Biophysical Journal* **57**, 507a.

MCMANUS, O. B., BLATZ, A. L. & MAGLEBY, K. L. (1985). Inverse relationship of the durations of adjacent open and shut intervals for Cl and K channels. *Nature* **317**, 625–628.

MCMANUS, O. B., BLATZ, A. L. & MAGLEBY, K. L. (1987). Sampling, log binning, fitting, and plotting durations of open and shut intervals from single channels and the effects of noise. *Pflügers Archiv* **410**, 530–553.

MCMANUS, O. B. & MAGLEBY, K. L. (1986). The large conductance Ca-activated K channel: accounting for the Ca sensitivity. *Biophysical Journal* **49**, 171a.

MCMANUS, O. B. & MAGLEBY, K. L. (1988). Kinetic states and modes of single large-conductance calcium-activated potassium channels in cultured rat skeletal muscle. *Journal of Physiology* **402**, 79–120.

MCMANUS, O. B. & MAGLEBY, K. L. (1989). Kinetic time constants independent of previous single-channel activity suggest Markov gating for a large-conductance Ca-activated K channel. *Journal of General Physiology* **94**, 1037–1070.

MCMANUS, O. B., WEISS, D. S., SPIVAK, C. E., BLATZ, A. L. & MAGLEBY, K. L. (1988). Fractal models are inadequate for the kinetics of four different ion channels. *Biophysical Journal* **54**, 859–870.

MAGLEBY, K. L. & PALLOTTA, B. S. (1983*a*). Calcium-dependence of open and shut interval distributions from calcium-activated potassium channels in cultured rat muscle. *Journal of Physiology* **344**, 585–604.

MAGLEBY, K. L. & PALLOTTA, B. S. (1983*b*). Burst kinetics of single calcium-activated potassium channels in cultured rat muscle. *Journal of Physiology* **344**, 605–623.

MAGLEBY, K., L. & WEISS, D. S. (1990*a*). Estimating kinetic parameters for single channels with simulation. A general method that resolves the missed event problem and accounts for noise. *Biophysical Journal* **58**, 1411–1426.

MAGLEBY, K. L. & WEISS, D. S. (1990*b*). Identifying kinetic gating mechanisms for ion channels by using two-dimensional distributions of simulated dwell times. *Proceedings of the Royal Society* B **241**, 220–228.

MARTY, A. (1981). Ca-dependent K channels with large unitary conductance in chromaffin cell membranes. *Nature* **291**, 497–500.

MARTY, A. (1983). Blocking of large unitary calcium-dependent potassium currents by internal sodium ions. *Pflügers Archiv* **396**, 179–181.

METHFESSEL, C. & BOHEIM, G. (1982). The gating of single calcium-dependent potassium channels is described by an activation/blockade mechanism. *Biophysics of Structure and Mechanism* **9**, 35–60.

MILLHAUSER, G. L., SALPETER, E. E. & OSWALD, R. E. (1988). Diffusion models of ion-channel gating and the origin of power-law distributions from single-channel recording. *Proceedings of the National Academy of Sciences of the USA* **85**, 1503–1507.

MOCZYDLOWSKI, E. & LATORRE, R. (1983). Gating kinetics of Ca^{2+}-activated K^+ channels from rat muscle incorporated into planar lipid bilayers: evidence for two voltage-dependent Ca^{2+} binding reactions. *Journal of General Physiology* **82**, 511–542.

MONOD, J., WYMAN, J. & CHANGEUX, J.-P. (1965). On the nature of allosteric transitions: a plausible model. *Journal of Molecular Biology* **12**, 88–118.

OBERHAUSER, A., ALVAREZ, O. & LATORRE, R. (1988). Activation by divalent cations of a Ca^{2+}-activated K^+ channel from skeletal muscle membrane. *Journal of General Physiology* **92**, 67–86.

PALLOTTA, B. S. (1985). Calcium-activated potassium channels in rat muscle inactivate from a short-duration open state. *Journal of Physiology* **363**, 501–516.

PALLOTTA, B. S., MAGLEBY, K. L. & BARRETT, J. N. (1981). Single channel recordings of Ca^{2+}-activated K^+ currents in rat muscle cell culture. *Nature* **293**, 471–474.

RAO, C. R. (1973). *Linear Statistical Inference and Its Applications*. John Wiley, New York.

SCHWARZ, G. (1978). Estimating the dimension of a model. *Annals of Statistics* **6**, 461–464.

SINGER, J. J., WALSH, J. V. JR (1987). Characterization of calcium-activated potassium channels in single smooth muscle cells using the patch-clamp technique. *Pflügers Archiv* **408**, 98–111.

VERGARA, C. & LATORRE, R. (1983). Kinetics of Ca^{2+}-activated K^+ channels from rabbit muscle incorporated into planar lipid bilayers: evidence for a Ca^{2+} and Ba^{2+} blockade. *Journal of General Physiology* **82**, 543–568.

WEISS, D. S. & MAGLEBY, K. L. (1989). Gating scheme for single GABA-activated Cl^- channels determined from stability plots, dwell-time distributions, and adjacent-interval durations. *Journal of Neuroscience* **9**, 1314–1324.

WONG, B. S., LECAR, H. & ADLER, M. (1982). Single calcium-dependent potassium channels in clonal anterior pituitary cells. *Biophysical Journal* **39**, 313–317.

YELLEN, G. (1984). Ionic permeation and blockade in Ca^{2+}-activated K^+ channels of bovine chromaffin cells. *Journal of General Physiology* **84**, 157–186.